UNIVERSITY OF ALBERTA

THE LIMITATIONS OF CCD CAMERAS IN THE MEASUREMENT OF SCOLIOTIC DEFORMITIES

BY

Kimberley Dawn Adams

A thesis submitted to the Faculty of Graduate Studies and Research in partial fulfilment of the requirements for the degree of Master of Science.

DEPARTMENT OF ELECTRICAL ENGINEERING

Edmonton, Alberta

SPRING 1993

National Library
of Canada

Acquisitions and
Bibliographic Services Branch

395 Wellington Street
Ottawa, Ontario
K1A 0N4

Bibliothèque nationale
du Canada

Direction des acquisitions et
des services bibliographiques

395, rue Wellington
Ottawa (Ontario)
K1A 0N4

Your file Votre référence

Our file Notre référence

The author has granted an irrevocable non-exclusive licence allowing the National Library of Canada to reproduce, loan, distribute or sell copies of his/her thesis by any means and in any form or format, making this thesis available to interested persons.

L'auteur a accordé une licence irrévocable et non exclusive permettant à la Bibliothèque nationale du Canada de reproduire, prêter, distribuer ou vendre des copies de sa thèse de quelque manière et sous quelque forme que ce soit pour mettre des exemplaires de cette thèse à la disposition des personnes intéressées.

The author retains ownership of the copyright in his/her thesis. Neither the thesis nor substantial extracts from it may be printed or otherwise reproduced without his/her permission.

L'auteur conserve la propriété du droit d'auteur qui protège sa thèse. Ni la thèse ni des extraits substantiels de celle-ci ne doivent être imprimés ou autrement reproduits sans son autorisation.

ISBN 0-315-82218-X

Canada

UNIVERSITY OF ALBERTA

RELEASE FORM

Name of Author:	Kimberley Dawn Adams
Title of Thesis:	The Limitations of CCD Cameras in the Measurement of Scoliotic Deformities
Degree:	Master of Science
Year this Degree Granted:	1993

Permission is hereby granted to THE UNIVERSITY OF ALBERTA LIBRARY to reproduce single copies of this thesis and to lend or sell such copies for private, scholarly or scientific research purposes only.

The author reserves other publication rights, and neither the thesis nor extensive extracts from it may be printed or otherwise reproduced without the author's written permission.

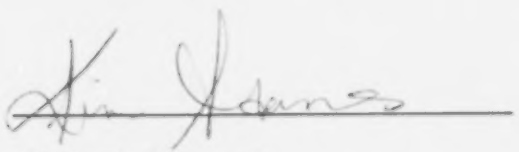

(Student's Signature)

Permanent Address:

302-10015 85 Avenue

Edmonton, Alberta, T6E 2J9

Date: Apr 21 '93

UNIVERSITY OF ALBERTA

FACULTY OF GRADUATE STUDIES AND RESEARCH

The undersigned certify that they have read, and recommend to the Faculty of Graduate Studies and Research for acceptance, a thesis entitled "THE LIMITATIONS OF CCD CAMERAS IN THE MEASUREMENT OF SCOLIOTIC DEFORMITIES" submitted by KIMBERLEY DAWN ADAMS in partial fulfilment of the requirements for the degree of MASTER OF SCIENCE.

N.G. Durdle

V.J. Raso

A.E. Peterson

K.A. Stromsmoe

Date: April 16/93

ABSTRACT

Digital video cameras and image capture hardware combinations have made the transfer of visual information to computers a simple but powerful procedure. Surface topography measurement systems have been developed based on CCD video cameras to monitor the progression of spinal deformities. Non-invasive surface topography measurements, if accurate enough, provide quantitative information about the deformities. The limitations on the accuracy of a CCD-based measurement system were analyzed.

The overall system distortion was determined by imaging a known control field. The overall system resolution was measured using a line pairs chart. The effects on distortion and resolution due to lens abberations were evaluated. The CCD image sensor was analyzed with respect to limitations on accuracy due to geometry. Sensor linearity, bloom, uniformity, and spectral response were also investigated to determine their effect on distortion and resolution. The overall system distortion, in object space, was 5.4 mm maximum at the periphery of the image. Overall system resolving power was 34 line pairs/mm at the sensor surface. The most significant contributors to system inaccuracy were lens barrel distortion (3.1 mm), lens diffraction (0.5 mm), and sensor space variancy (0.5 mm). Digitizing irregular shapes into a regular array and sensor device characteristics impose inaccuracies to a lesser extent, between 0.1 mm and 0.5 mm. Barrel distortion of the lens and non-uniformity of the CCD sensor are systematic errors which can be removed.

Based on the results of this analysis several recommendations are made to improve the accuracy of surface topography measurement systems which use CCD video cameras.

ACKNOWLEDGEMENTS

I would like to thank my supervisors, Nelson Durdle and Jim Raso, for their support and guidance throughout my graduate program.

Many people at the Glenrose Hospital gave me support in the way of advice, assistance, and encouragement. In particular, I would like to thank the departments of Seating, Maintenance, Security and Audio Visual Services and the individuals Doug and Shelly.

I would also like to thank the staff and graduate students in the Electrical Engineering department who so generously offered their time, especially Blair, Mak, the Machine Shop, and the Alberta Microelectronics Centre. Thanks also go to Dr. Fedosejovs, Jim Fern and Kees DenHartigh who loaned me equipment for my experiments.

Finally, thanks to my family for their wonderful support and encouragement during this "mammoth task". I am especially grateful to Kevin, "the artist", who made some diagrams for me.

TABLE OF CONTENTS

CHAPTER ONE: INTRODUCTION 1

1.1 Purpose 1

1.2 Motivation 1

1.3 Overview 2

CHAPTER TWO: BACKGROUND 4

2.1 Scoliosis 4

2.2 Assessment Techniques 5

2.3 Video Camera Image Capture System 12

2.3.1 Object in Scene 13

2.3.2 Lens 13

2.3.3 CCD Array Image Sensor 15

2.3.4 Signal Processing 24

2.3.5 Signal Transmission 25

2.3.6 Frame Grabber 25

2.3.7 Image Processing 27

2.4 Summary 27

CHAPTER THREE: OVERALL DISTORTION AND RESOLUTION ... 29

3.1 Overall System Distortion 29

3.2 Aspect Ratio 36

3.3 Overall System Resolution 38

CHAPTER FOUR: SENSOR CHARACTERISTICS 41

4.1 Background on Experimental Setup 41

4.2 Spectral Response 47

4.3 Linearity 49

4.4 Saturation Voltage 54

4.5 Quantization 54

4.6 Bloom 58

4.7 Uniformity 64

4.8 Summary 66

CHAPTER FIVE: INDIVIDUAL ERRORS 67

5.1 Lens 67

5.2 Sensor Geometry 71

5.3 Sensor Characteristics 78

5.4 Camera Circuitry 85

5.6 Summary 86

CHAPTER SIX: RECOMMENDATIONS AND CONCLUSIONS 88

6.1 Recommendations 88

6.2 Conclusions 94

6.3 Future Work 95

REFERENCES 97

LIST OF TABLES

Table 3.1: Maximum Distortion in Pixels. 34

Table 4.1: Summary of Sensor Characteristics 66

LIST OF FIGURES

Figure 2.1: Grid of Raster Points on the Back Surface 9

Figure 2.2: Block Diagram of Surface Topography Measurement System .. 11

Figure 2.3: Transfer of Charge Packets 20

Figure 3.1: Layout for Determination of Overall Distortion and Resolution 30

Figure 3.2: Error Vector Diagram 35

Figure 3.3: Image Aspect Ratios 37

Figure 4.1: Logarithmic Current Drive Circuit Schematic 44

Figure 4.2: Spectral Response of Image Sensor 48

Figure 4.3: Optical Setup for Linearity Determination 50

Figure 4.4: CCD Sensor Response for Linearity Determination 55

Figure 4.5: Video Signal Response for Linearity Determination 56

Figure 4.6: Optical Setup for Bloom Determination 59

Figure 4.7: Sensing Element Response for Bloom Determination 62

Figure 4.8: Video Signal Response for Bloom Determination 63

Figure 5.1: Continuous Image Transformed into Discrete Space 74

Figure 5.2: Non-Linearity Effects on Centroid Calculation 81

Figure 5.3: Quantization Level Effects on Centroid Calculation and

Resolving Power 83

LIST OF SYMBOLS AND ABBREVIATIONS

A	Sensor output amplitude
c	Speed of light
C	Circle of confusion
C_{ox}	Capacitance per unit area of the oxide
d	Diameter of beam
d_{diff}	Diffraction limited diameter of focal point
diam	Diameter of focal point
E_g	Band gap energy
E_I	Ionization energy
EPX	Effective digitized pixel size in x direction
EPY	Effective digitized pixel size in y direction
f	Focal length
g	Spatial frequency of image
g_o	Spatial frequency of CCD sensing elements
GRH	Glenrose Rehabilitation Hospital
h	Hyperfocal distance
H	Horizontal sensor size
hv	Energy of a single photon
i	Current
I	Intensity of radiation
IC	Integrated circuit

M	Magnification factor
MOS	Metal Oxide Semiconductor
MTF	Modulation Transfer Function
n	Semiconductor material doped with impurities with extra electrons
N	F-number
NH	Number of horizontal CCD sensing elements
NTSC	National Television System Committee
NV	Number of vertical CCD sensing elements
p	Semiconductor material doped with impurities with extra holes
pixel	Picture element
PH	Effective digitized horizontal image size
PV	Effective digitized vertical image size
Q_{INV}	Charge of inversion layer
r	radius
R	Resistance
s_x	Size of sensing element in x direction
s_y	Size of sensing element in y direction
sel	Sensing element
V	Vertical sensor size
V_G	Gate electrode voltage
V_{th}	Gate electrode threshold voltage
VLSI	Very Large Scale Integration
w_o	Beam waist

σ_b^2	Mean square boundary location error
σ_c	Error of x coordinate centre estimate
Θ	Beam divergence
ϕ_s	Surface potential
λ	Wavelength
λ_{co}	Cut-off wavelength

CHAPTER ONE: INTRODUCTION

1.1 Purpose

The objective of this thesis was to determine the limitations of Charge-Coupled Device (CCD) cameras when used for topographical studies of spinal deformity. This thesis describes the video system in place at the Glenrose Rehabilitation Hospital and presents background information on image capture systems which use CCD cameras. The sources of error are investigated and classified as systematic, or, non-systematic. Recommendations are made regarding the use of CCD cameras for topographical studies.

1.2 Motivation

Digital video camera and image capture hardware combinations have made the transfer of visual information to computers a simple but powerful procedure. At the Glenrose Rehabilitation Hospital, three video cameras (JVC TK-S310U: JVC, Japan) image an array of light spots projected onto a subject's back, the images are digitally captured on a computer, and the image data are transformed into three dimensional coordinate data. This information is used to map the topography of the back and

document changes in trunk deformities. It was necessary to define the accuracy of this system to ensure perceived topographical changes were due to actual trunk change rather than system inaccuracy. CCD cameras are used in many applications and are cited as being highly accurate, yet, this may not be the case. An analysis of each stage of the image capture system was needed to determine how the accuracy of the system could be improved.

1.3 Overview

Specifically, the objectives of this work were to determine the accuracy and resolution of CCD cameras for qualitative imaging and to quantify sources of errors and establish their relative importance.

Experiments to determine overall video system accuracy were performed using standard known images to measure the degree and type of distortion across the image field and camera resolution.

The overall error is a sum of elementary errors which are individually independent but may occur consistently (El-Hakim et al., 1987). Elementary errors can be introduced at any stage of the image capture system: the object in the scene, lens, CCD array, signal processing, signal transmission, or frame grabber. The proportion

of the overall system error due to lens abberations were analyzed. The geometrical errors due to array sensing element size and placement were determined. Errors involved in the digitization of continuous functions into discrete elements were quantified. Sensor characteristic response to incident light intensity was investigated; experiments were developed to determine spectral response, linearity, saturation illumination, bloom, and uniformity. To obtain these response characteristics a laser source was optically coupled to a CCD sensing element. Characteristics which contribute to overall error in point location were discussed. The signal processing, signal transmission, and image processing stages of a video image capture system were briefly discussed with respect to overall distortion.

Errors which can be eliminated by calibration routines at the image processing stage were identified.

CHAPTER TWO: BACKGROUND

2.1 Scoliosis

Scoliosis involves a lateral bend and an axial rotation of the spine. Idiopathic scoliosis, meaning "spinal curvature without a known cause", can occur at any age, adolescence being the most common (Glanze, 1985). It can occur in both genders, however, it mostly occurs in females. Besides the spine curvature more subtle physical signs of scoliosis are: unlevel shoulders and hips; a prominent shoulder blade, breast, flank area or hip; and apparently poor posture. Physiological signs of scoliosis are fatigue and decreased lung function for very severe deformities.

Little is known about the cause of idiopathic scoliosis, but, it is generally felt that it results from more than one factor (Burwell, 1992). There are several physiological anomalies in skeletons, neuromuscular tissues, hormones, and collagen associated with scoliosis, but, whether they are the cause or the effect has not been determined.

Bony tissue is rigid, but, malleable and undesirable pressures cause permanent deformations. Gravity, growth, and muscle forces act on vertebra to deform them while the upright human trunk searches for a "conus of economy", ie. an ability to balance with an economy of effort (Dubousset, 1992; Burwell, 1992).

Since so little is known about its cause there is no preventative treatment for idiopathic scoliosis. Once discovered, there are treatment measures, such as, bracing, casting, and corrective surgery. Casts and braces should apply a derotation force rather than a distraction force. However, their success is questionable. Surgery, on extreme curvatures, involves attaching rods to vertebrae to apply an axial distraction force and/or rotational forces.

2.2 Assessment Techniques

Images of the spine and back surface must be taken repeatedly over time to track progression of the curve, to determine when bracing/surgical intervention is necessary and whether intervention has been beneficial. Presently, the documentation of spinal deformity over time is inadequate (Burwell, 1992).

Measurement techniques should reflect the fact that scoliosis is a three dimensional deformity. Complete determination of scoliosis requires three dimensional measurement of both the spine and the back surface. As early as 1865, Adams was recording three dimensional information by taking plaster casts of patient's backs (Adams, 1865). However, with the advent of radiography, a bidimensional mentality was adopted for measuring and tracking scoliosis (Dubousset, 1992). Today, the three-dimensional approach has resurfaced.

To obtain three dimensional images of the spine itself, bi-plane radiography (two radiographs taken from different angles), computed tomography (CT) and magnetic resonance imaging (MRI) are used. CT and MRI are limited clinically; CT because of the radiation dosage and MRI because of the expense (Drerup, 1992).

To obtain back surface measurements several methodologies are available, including ultrasound, tactile, and goniometry, however, optical methods are the most widely accepted (Drerup, 1992). In moiré topography, a patient is illuminated by a point source through a grating. When observed through the same grating, interference fringes appear on the back surface. These fringes, moiré fringes, represent contours of distance 3-5 mm, depending on the grating, and points on the back surface can be measured to a resolution of 0.5 mm (Drerup, 1992). However, this method is subject to large errors due to changes in the fringe pattern resulting from patient movement. In addition, it is difficult to use computerized acquisition and analysis approaches because of the irregular pattern of fringes.

In another optical method, a pattern of lines or dots is projected onto the back surface and an image is taken. When using line patterns, either multiple parallel lines are projected onto the back surface and recorded in a single frame (Frobin & Hierholzer, 1981 and 1983), or, a single line is projected onto the back surface and increments across the back are recorded in multiple frames (Turner-Smith, 1986). After the images have been obtained, two dimensional coordinate information is

extracted and three dimensional coordinates are calculated.

Surface topography analysis is important because exterior appearance is what the patient and the parents notice and want to improve. Clinically, several techniques are available which measure the rotation, pattern and magnitude of the curve. The advantages of using video surface topography methods instead of radiography to derive these measurements are safety and cost. The visible light source is hazard free for both operator and patient, and once set up, the running cost is 1/100 of an equivalent radiograph (Quantec Spinal Measurement System, Emilcott Associates, Inc., Madison, NJ). However, there is much debate as to whether skeletal information can actually be derived from the topographical map of the back.

The question is not, whether surface topography can give the same measurements as radiography, but, can it give an accurate three-dimensional reconstruction of the spine (Hierholzer & Drerup, 1992)? The two methods have complementary uses. Radiography gives a picture of the spine, whereas, surface topography gives a three dimensional picture of the surface deformity. Some replacement of radiographs is possible for shape and curvature analysis if the user is only generally interested in the spinal midline, but, the degree of accuracy of the image must be defined (Drerup, 1992). Local shape analysis requires at least 1 point/cm^2, a large set of data points, and curvature analysis requires at least 0.2 mm accuracy, a very precise measurement (Drerup, 1992). Most measurement systems fail to meet these requirements.

In Japan, Suzuki et al. (1992) extract information from moiré surface topography images to detect the degree of spinal deformity and to detect progression. They used the height of the hump at three levels of the back to express deformity and concluded that the surface measurement was reliable for the follow-up of mild scoliosis. They have had no cases where this method failed to detect progression.

Surface images of the human back are used at the Glenrose Rehabilitation Hospital (GRH) to monitor spinal deformities. Previously, these images were obtained using a moiré fringe pattern method developed by Rodger (Rodger, 1980). With this system a point on the back could be determined with an accuracy of ±4 mm (Wegner, 1985). The time required for special film processing and manual digitization of fringe data precluded using the results in treatment decisions. A video based technique, which is faster and more accurate, has been developed at the GRH to replace the moiré method (Slupsky, 1988; Hill, 1990 and 1992). This system is based on a rasterstereography method described by Frobin and Hierholzer (1981) in which a grid of light points is projected onto the body surface (Figure 2.1). Frobin and Hierholzer used a solid state camera with a linear image sensor oriented in the y coordinate direction and a motor driven translator to move the camera in the x direction. Since that time solid state charge coupled device (CCD) cameras with array image sensors have become widely used.

The GRH system consists of three video cameras (JVC TK-S310U) with 16 mm F/1.4

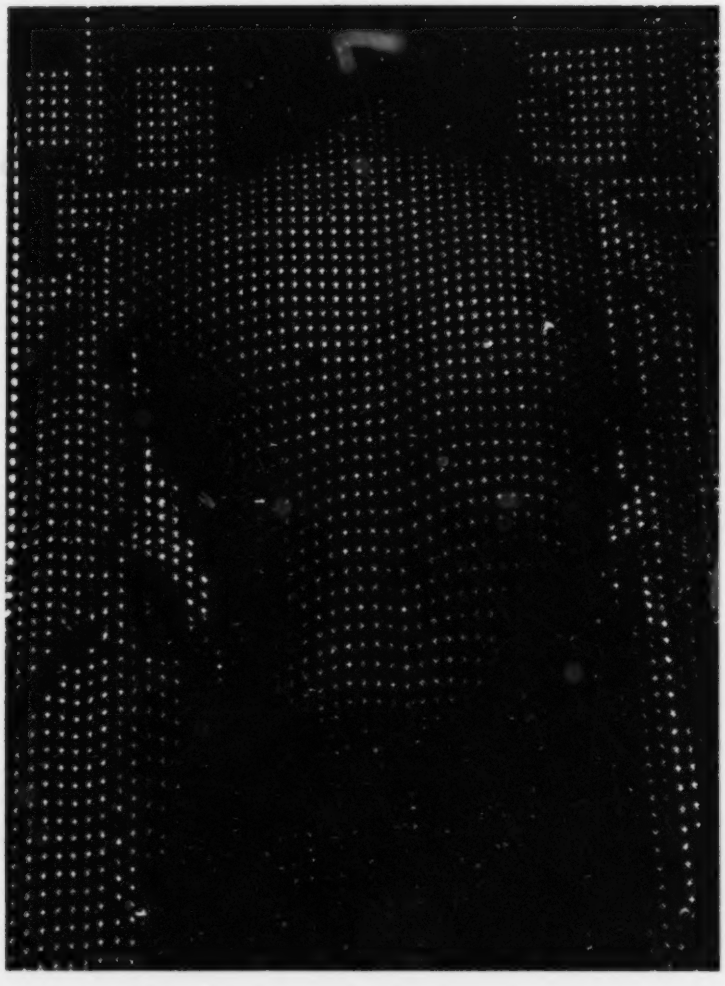

Figure 2.1: Grid of Raster Points on the Back Surface

lenses and a Scion Image Capture II real time frame grabber (Figure 2.2) (Hill, 1990). Images are analyzed on a Macintosh II computer using an image capture program, "Image" (Rasband, 1990), and on an IBM RISC station with custom software. The image sensor, a Hitachi HE98246 Transversal Signal Line Image Sensor, has an area of 8.8 by 6.6 mm^2 with 649 by 491 effective sensing elements (sels). The frame grabber has 640 by 480 picture elements (pixels) with 8 bit grey level resolution.

Centroids of the light spots are calculated for the three images. Then, the light spots in each image are correlated. The three sets of two dimensional centroid locations are used to determine the three dimensional x, y, and z coordinate of each light spot. Calculation of these coordinates incorporates camera calibration parameters to increase their accuracy. A topographical map of the back surface is constructed using these three dimensional coordinates. These maps are used to document the progression of the deformity, to determine when to intervene with treatment and to determine treatment effect. To be useful as a diagnostic tool the accuracy of the system must be defined to determine if perceived topographical changes are due to actual trunk change or system inaccuracy. Initial studies indicate that the video based technique has a spatial coordinate accuracy of 2 to 5 mm (Hill, 1990). The accuracy of the GRH surface topography system should be improved to 0.2 mm before curvature analysis can be performed with confidence (Drerup, 1992). Further drawbacks of the GRH surface topography system are poor quality images, especially

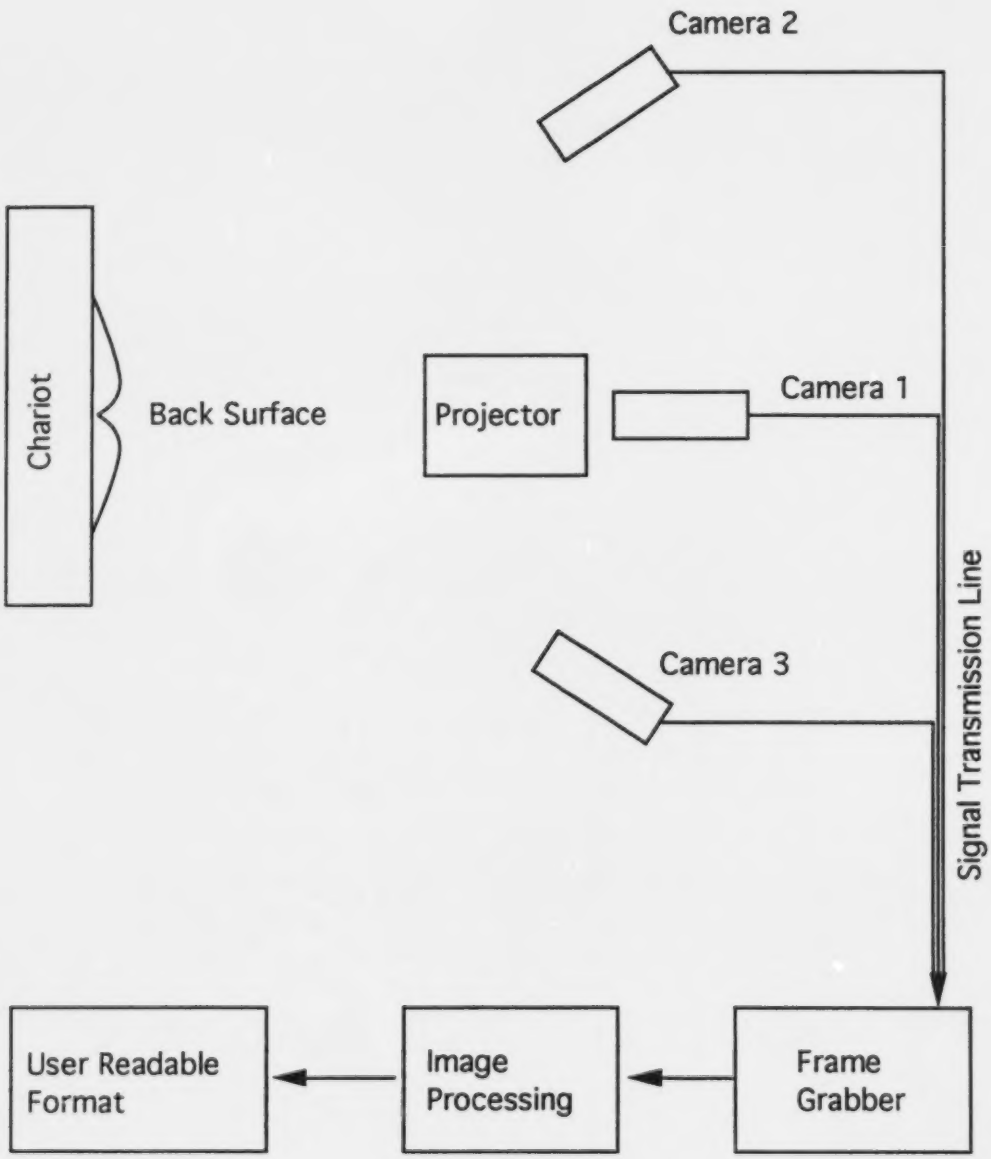

Figure 2.2: Block Diagram of Surface Topography Measurement System

on the side views, and considerable time and labour required for the manual digitization of control points for the correlation program.

2.3 Video Camera Image Capture System

Many applications use CCD sensors to extract three dimensional measurements because they are considered to be very accurate, stable, of small size, and rugged (El Hakim, et al., 1989). For example CCDs are used: in industrial settings (Tsai, 1987; Zhang and Liang, 1989; Butler & Pierson, 1991; Kaida, et al., 1990), for star tracking (Hopkinson, et al., 1987), for particle detection (Damerell, et al., 1986), and for biomedical imaging (Fedotov, et al., 1989; Cholewicki, et al., 1991). In particle detection, Damerell found spatial precision of their CCD to be 5 μm (Damerell, et al., 1980; Bailey, et al., 1982; Damerell, et al., 1986). Li et al. (1989) found measurement errors can be reduced to 0.1 subpixel accuracy following calibration.

A video image capture system consists of several stages: the object in the scene, lens, image sensor, signal processing, signal transmission, frame grabber and image processing. This section discusses the basic functions and errors associated with the lens and the CCD image sensor only. Although the remaining stages also introduce errors, they are not within the scope of this study, however, a brief background is presented for completeness.

2.3.1 Object in Scene

Optimum lighting conditions are required to produce a high quality image which is essential when extracting geometric information (Cholewicki et al., 1991; Fryer & Mason, 1989; Havelock, 1989; Ho, 1983). Hill (1990) found that image quality is a problem in surface topography measurements since contrast between background and light points must be maximized, but excessive light caused blooming. Low light levels make visual information hard to discern from noise and high light levels make boundaries of bright objects increase in size because of blooming. Proper and consistent positioning of the patient is also a concern in the documentation of spinal deformities over time. A "chariot" frame was built for the GRH surface topography measurement system which supports the patient (Wegner, 1985).

2.3.2 Lens

An optical system of lenses focuses the image of an object onto the front face of the image sensor. There are several laws which govern the pathway of light through an optical system. Light rays do not always focus where expected, because lenses have abberations due to material or manufacturing imperfections. Several types of lens abberations are (SPIE, 1965; Welford, 1991; Horder, 1973):

1. Spherical: Light rays through the edge of the lens focus nearer to the lens

than rays through the centre.

2. Chromatic: Light of different wavelengths is magnified differently. In addition, light of different wavelengths have different indices of refraction in the same medium; short wavelengths focus closer to the lens than long wavelengths.

3. Coma: For a point source which is off-axis, light rays travelling through the centre of the lens focus further from the optical axis than light rays travelling through the edges of the lens.

4. Astigmatism: Rays of light in the vertical plane do not focus to the same point as those from the horizontal plane.

5. Curvature of field: Images of objects focus on a curved surface rather than a focal plane.

6. Distortion: The magnification factor at the edge of a lens is different than it is at the centre of the lens. If axial magnification is greater than off-axis magnification the lens has positive, or barrel, distortion. If axial magnification is less than off-axis magnification the lens has negative, or pincushion, distortion.

7. Diffraction: Light passing close to the edge of an opaque obstacle, like a narrow aperture, causes a focal point to be transformed into a circle of light, called an Airy disc.

Lens abberations distort the imaged location of points which are used to extract

measurement information from visual pictures (Sid-Ahmed, et al., 1990; T. R. Little, 1977; Lenz & Fritsch, 1990). Some lens abberations, like distortion, can be considered in camera calibration algorithms to improve the accuracy of the position measurement. A lens can be "stopped down" (decrease the aperture diameter) to reduce chromatic, coma, curvature of field and spherical abberations (Hutber, 1987). Other abberations, like diffraction and defocussing are non-systematic (Hutber, 1987; Lenz & Fritsch, 1990).

2.3.3 CCD Array Image Sensor

The concept of the Charge-Coupled Device (CCD) was proposed by Boyle and Smith in 1970 as an electrical substitute for magnetic bubble devices using metal-oxide-semiconductor (MOS) integrated circuit technology (Boyle & Smith, 1970). Four years later a 320 x 512 bit image sensor using the CCD concept was developed (Rodgers, 1974). Before that, imaging was performed using solid-state imagers with an integrated matrix of addressable photodiodes. The number of resolvable points using CCD imagers surpassed that of photodiode matrices causing CCD imagers to become more popular.

A CCD array image sensor translates visual information into a two dimensional electrical representation of a scene. CCD array image sensors are integrated circuits

with an array of light sensitive elements (sensor elements, sels). Incoming light photon energy is translated into electron-hole pairs. When an electrode of the CCD is held at a positive voltage these photon induced electrons are attracted to it (El-Hakim, et al., 1989; Sedra, et al., 1982). The charge packet gathered at the electrode is proportional to the number of photons entering the silicon (ie. the local light intensity). The packet is shifted to a storage site, and manipulating electrode voltages with a clocking system shifts the stored charge sequentially along the row of electrodes like a shift register (Hopkinson, 1982, and Sedra, et al., 1982). At this stage, the signal is analog since charge packets store a variable, not digital, amount of charge. These analog potentials are sampled, and then mapped serially onto a single line one pixel at a time.

There are several physical principles which govern the aforementioned functions. CCD image sensor integrated circuits are fabricated on semiconductor material, typically silicon. Semiconductor material absorbs electromagnetic radiation, ie. light photons. Silicon is particularly receptive to near-infrared wavelengths, but, is commonly used for visual imaging (Beynon & Lamb, 1989; El-Hakim, et al., 1989).

Absorption of electromagnetic radiation causes electrons to transfer states. In one type of state transfer an electron-hole pair is produced when photons possess enough energy to excite an electron across the band gap from the valence band to the conduction band. Thus, a hole in the valence band and an electron in the conduction

band are generated, an electron-hole pair. Absorption leading to this type of state transfer is called intrinsic absorption. There is strong absorption of electromagnetic radiation at short wavelengths up to a cut-off wavelength given by the Planck relationship:

$$\lambda_{co} = \frac{hc}{E_g} = \frac{1.24}{E_g}(\mu m)$$

(Eq. 2.1)

where, h = 4.14×10^{-15} eV, c = 3.00×10^{8} m/s, and E_g is the band gap energy. This relationship only holds for direct band gap materials, ie. material in which the lowest conduction band and highest valence band energies occur at the same value of electron momentum. Otherwise, the cut-off wavelength is not so easily defined.

Visible light consists of wavelengths ranging from 0.4 to 0.7 μm. Silicon has a peak sensitivity at approximately 0.8 μm and relatively good sensitivity down to 0.4 μm. Its band gap energy is 1.12 eV, thus, the cut-off wavelength is approximately given by:

$$\lambda_{co} = \frac{1.24}{1.12} = 1.11 \mu m$$

In another type of state transfer either a hole is generated in the valence band or an electron is generated in the conduction band. This is accomplished with impurities in the material which act as acceptor sites for electrons transferring from the valence

band, or, as donors of electrons to transfer to the conduction band. Electromagnetic radiation absorption leading to this type of state transfer is called extrinsic absorption. Ionization energy, E_I, is the difference in energy between the impurity level and the band edge (either the conduction band for donors or the valence band for acceptors). In this case, cut-off wavelength is given by:

$$\lambda_{co} = \frac{hc}{E_I} = \frac{1.24}{E_I}(\mu m)$$

(Eq. 2.2)

Consequently, a particular cut-off wavelength can be attained by doping semiconductor material with impurities with the required ionization energy. Intrinsic absorption is more efficient than extrinsic absorption, but, both methods lead to the production of electrons in the conduction band and holes in the valence band.

Prior to the application of an electrode voltage, there is a uniform distribution of holes in the p-type semiconductor. When a voltage is applied at the gate electrode, holes are repelled from the area beneath it, creating a region called the depletion layer. The larger the potential applied at the electrode the larger the depletion layer, until, the potential at the semiconductor/insulator interface becomes so positive that electrons are attracted to the interface. The gate potential at which this occurs is called the threshold voltage, V_{th}. Electrons at the interface form an inversion layer which is thin, but, very dense. This inversion layer is analogous to the channel created in MOS transistors, hence the name, n-channel CCD. MOS transistors have

an ample supply of minority carriers from the source and/or drain, however, in CCDs there is no such supply so an inversion layer cannot form immediately. If there is no inversion layer the depletion layer extends much further into the bulk semiconductor. The charge storing potential, the "potential well", of the depletion layer increases linearly with the applied gate voltage, and decreases linearly with the charge density of the inversion layer.

Electrodes are spaced closely together on a CCD structure. Initially, all electrodes are biased in excess of the threshold voltage so they all have potential wells under them. If one of the wells is biased much higher than threshold then the potential well below it becomes much deeper than the others, thus, charge is attracted to it. Figure 2.3 depicts how charge is transferred along the CCD structure. If the bias of the electrode next to the first well becomes high, then the potential well below it deepens and the charge packet distributes between the two wells. When the potential at the first electrode returns to the resting threshold voltage, its well collapses and the charge packet concentrates in the deep well. By applying potentials in succession, the charge packet propagates along all the device.

An external line to each of the electrodes on the device is impractical so electrodes are grouped together. Each group is connected to a different clock. For a charge packet to propagate in only one direction, at least three phases are needed. Only two phases are needed if the device is constructed to physically restrict travel of

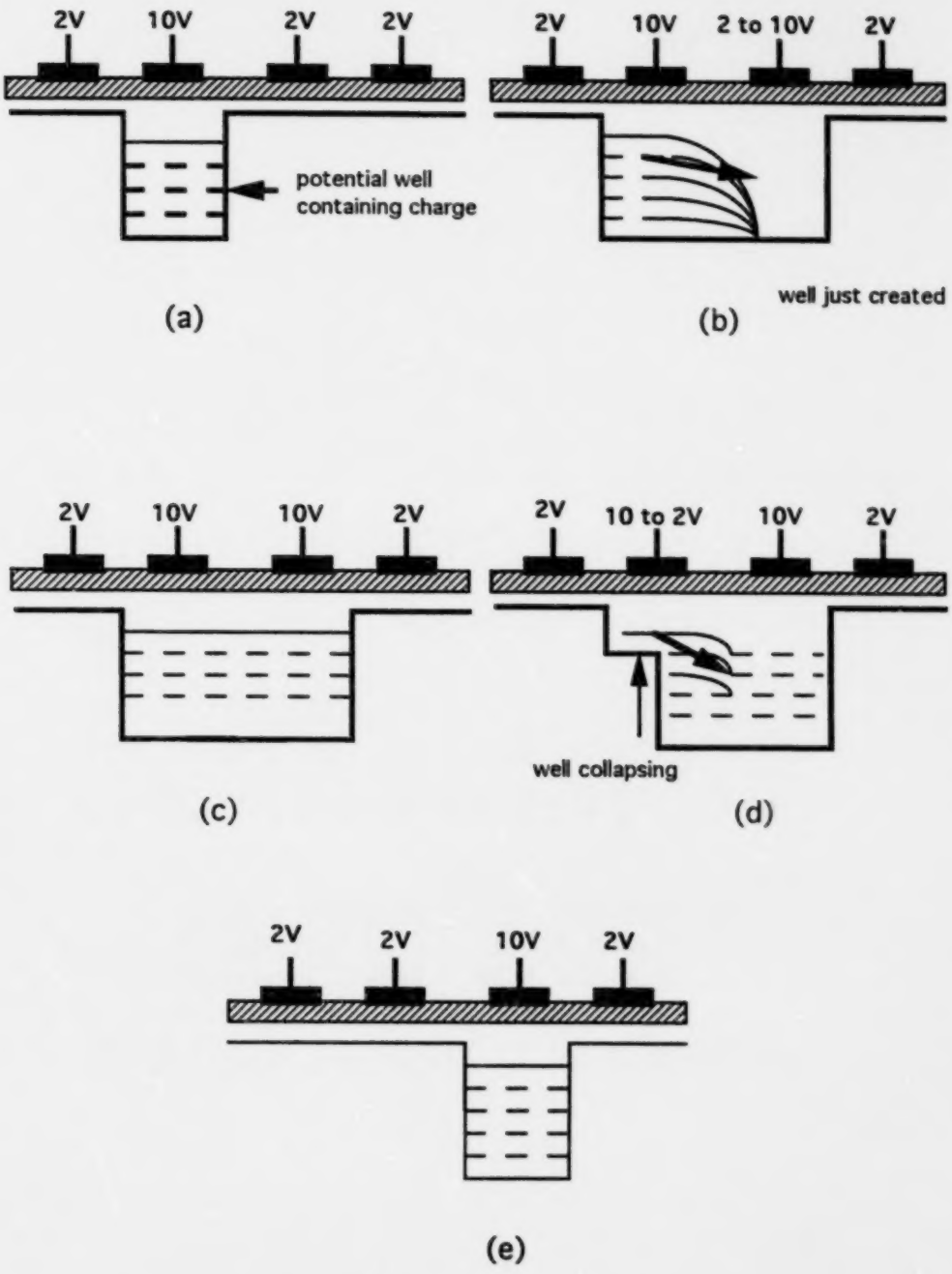

Figure 2.3: Transfer of Charge Packets

charge in the wrong direction.

The spacing of sensing elements can be expressed as a spatial frequency, g_o, in elements per mm. The spacing between maxima of intensity of the image that falls on the sensor can be expressed as spatial frequency, g, in line pairs per mm. The maximum image spatial frequency detectable by the sensor, its resolution, is limited at the Nyquist frequency, $g_o/2$. Modulation depth is the difference between maxima and minima at the CCD output when imaging a line pair. Modulation Transfer Function, MTF, which plots modulation depth as a function of image spatial frequency, decreases at high spatial frequencies. Geometric characteristics of CCD sensors which cause a fall off in MTF are: continuous space transformed into discrete spatial samples, spatial aliasing, and irregular sel spacing (Ho, 1983). These are discussed further in Chapter 5.

There are several electrical device characteristics that limit the performance of CCDs:

1) Inter-Electrode Gap. Exposed oxide surfaces in the inter-electrode gap can assume a potential which inhibits the transfer of charge packets between adjacent potential wells.
2) Lateral Confinement. Charge packets must be confined laterally to prevent spread of charge in the direction perpendicular to desired propagation.
3) Charge Handling Capacity. Ideally a CCD should have large output signals and small gate signals and sel dimensions. However, as the gate signal and sel

dimensions become smaller the charge packet size, Q_{INV}, also becomes smaller. This trade-off is seen in the following relationship (Beynon & Lamb, 1980):

$$Q_{INV} = C_{OX} V_G A$$

(Eq. 2.3)

Where Q_{INV} = the charge in the inversion layer (Coulombs), C_{ox} = the capacitance per unit area of the oxide (Coulombs/Volt per cm^2), V_G = gate voltage (Volts), and A = area of the gate (cm^2).

4) Charge Transfer. Charge packets are not transferred instantaneously or completely from one well to the next. If there is some charge remaining in a well as it collapses charges could drift in the wrong direction. Additional charge is lost when these minority carriers recombine with majority carriers.

5) Trapping. Trapping of electrons by surface states occurs at the silicon/silicon oxide (Si/SiO_2) interface in surface channel CCDs. Surface state energy varies widely as the CCD changes from deep depletion to inversion. If the surface state energy is below the Fermi level it will trap electrons from the conduction band. If the surface state energy is above the Fermi level it will re-emit electrons to the conduction band. If the time constant for the surface state is longer than that for the transfer of charge, trapped electrons will not be re-emitted until a following charge packet in the same, or subsequent, frame. This phenomenon is called a latent image. Indeed, this latent image can persist for several minutes (Epperson, 1987).

6) Smear. During the readout period, there is still light incident upon the sensor. Thus, charge packets transferring through the array will pick up more charge due to the new electron-hole pairs generated by the incoming radiation.

7) Bloom. There is a maximum number of charges a potential well can handle. If an overload occurs at one sensing element, charges spread outward towards neighbouring elements (Fedotov, et al., 1989; Hopkinson, 1987).

8) There are several other sources of noise in a CCD sensor:

a) Sensing noise. Usually, the most significant component is due to the resetting procedure.

b) Dark current. Minority carriers are generated continually and randomly by thermal effects (Hutber, 1987). Generation may not be uniform, however, since, dark current spikes generally occur at defects in the silicon (Tanikawa, et al., 1976).

c) Input photon noise. The generation of photons from an object is random, thus, the charge packet collected is not entirely indicative of the actual image. However, this is a fundamental limitation of all image sensors, not just CCDs.

d) Non-uniformity. There is a variation in size and spacing of sensor elements that cause charge handling capability to vary from one region to another. A multiplication factor can be incorporated into sampled data values to eliminate this effect (Little, 1977; Hutber, 1987; Ohnishi, et al., 1985).

2.3.4 Signal Processing

The output video camera signal is an NTSC standard video signal (Real, 1986; Kiver, 1955). Each line consists of image information and a horizontal synchronization pulse. Each field consists of 262.5 lines and a vertical synchronization pulse. One NTSC monochrome video frame consists of two interlaced fields, each consisting of 262.5 lines. When rebuilding the image from the video signal, the horizontal synchronization pulse resets the scanning to the left side of the image, and the vertical synchronization pulse resets the scan to the top left of the image. The vertical pulse contains information about which field should be displayed (uneven or even lines).

The signal emerges from the camera with a voltage potential which is proportional to the input light intensity but has losses due to the sensor and is altered due to internal processing by the camera. After leaving the CCD the analog signal representing the charge packet undergoes several processing stages before emerging from the camera as an NTSC standard signal: pre-amplification, D/A conversion, clamping, black offset, dark current compensation, blanking, clipping, vertical edge correction, aperture correction, filtering, and synchronization.

This signal processing can affect the resolution of digital cameras. In particular, filters have significant effect on the content of an image. Filters are used to prevent

aliasing, to limit the bandwidth, and to enhance edges. Although, a lowpass filter cannot avoid the aliasing caused by spatial sampling through the sensor, it does filter out noise and prevents further aliasing due to analog to digital conversion (Lenz and Fritsch, 1990). Filters used are usually low pass filters of a higher order which introduce a non-symmetric distortion in the image. In addition, filter overshoot causes shadows in the image (Dähler, 1987). Accuracy and definition of the horizontal synchronization pulse, warm up effects, resampling, aliasing, and voltage fluctuation are other sources of error at the signal processing stage (Dähler, 1987; Fryer & Mason, 1989).

2.3.5 Signal Transmission

The cable used for signal transmission is standard co-axial video quality cable with BNC and DB-15 connectors. Unfortunately, noise is introduced to the video information during transmission to the frame grabber (Hutber, 1987).

2.3.6 Frame Grabber

A frame grabbed image is a two dimensional array of digital grey level values representing the scene. The NTSC video signal information between horizontal

synchronization pulses is digitally converted into one line of the frame grabber array. Real time frame grabbers consist of an A/D converter and clocking and synchronizing circuitry to store one video frame in 1/30 sec and they may include very fast memory (Stanley, 1984).

Like spatial aliasing at the sensor, and aliasing at the signal processing stages, the frame grabber also introduces aliasing problems caused by undersampling a signal (Lenz & Fritsch, 1990; Dähler, 1987). Frequencies higher than the folding frequency overlap with the actual signal causing an erroneous output. Since the output of a camera contains high frequencies resulting from the D/A conversion, the signal bandwidth must be limited with a filter or the camera and frame grabber clocks must be identical. A slight hardware timing mismatch between image acquisition hardware and camera scanning hardware is another source of error. In a study by Tsai (1987), a 1% difference in synchronization signals caused an error of up to 5 pixels.

Even with no aliasing or timing mismatch, a significant loss of resolution occurs because the spatially quantised signal from the CCD is converted into a continuous analogue signal and then back to a quantised form by the frame grabber (Hutber, 1987). In addition, the CCD and frame grabber, usually, have different array sizes, and this mismatch further reduces resolution.

2.3.7 Image Processing

At this stage the data from the image is transformed into user readable form, for example, a three dimensional image or numerical calculations of area. Before being displayed, the image can be enhanced using three methods: geometric operations, pixel operations or neighbourhood operations (Stanley, et al., 1984). Calibration routines to eliminate distortions can also be performed at this stage.

2.4 Summary

The accuracy of the surface topography measurement system at the Glenrose Rehabilitation Hospital must be improved. There are many potential areas for distortion and loss of resolution, as presented in this chapter. The following chapters attempt to quantify the distortions from each stage of the surface topography system and determine if they are systematic.

Lens distortion and diffraction, sensor pitch, and signal processing are expected to have significant effects on distortion and resolution. CCD device characteristics were not expected to be as significant, however, this needed to be verified. Dark current, photon noise, charge handling capacity, and charge transfer efficiency of the sensor, and spherical, coma, astigmatism, and curvature of field abberations of the lens were

outside the scope of this research.

CHAPTER THREE: OVERALL DISTORTION AND RESOLUTION

Standard known charts were imaged to measure overall system distortion and resolution. The contribution to overall distortion and resolution limitation due to the lens and CCD sensor are examined in Chapter 5.

3.1 Overall System Distortion

A chart of known control points was imaged with the video camera system to determine the magnitude of total spatial distortion.

Materials and Methods

The equipment layout is shown in Figure 3.1. A JVC TK-S210U CCD video camera (JVC, Japan) with 649(Horizontal) by 491(Vertical) sels was used. Images were captured with a Scion Image Capture II board (Scion Corp., Walkersville, USA) in a Macintosh II computer (Apple Computer, Inc., Cupertino, USA), giving images of 640 by 480 pixels with 8 bit grey level resolution. Manual digitization was performed using "Image", image processing software (Rasband, 1990).

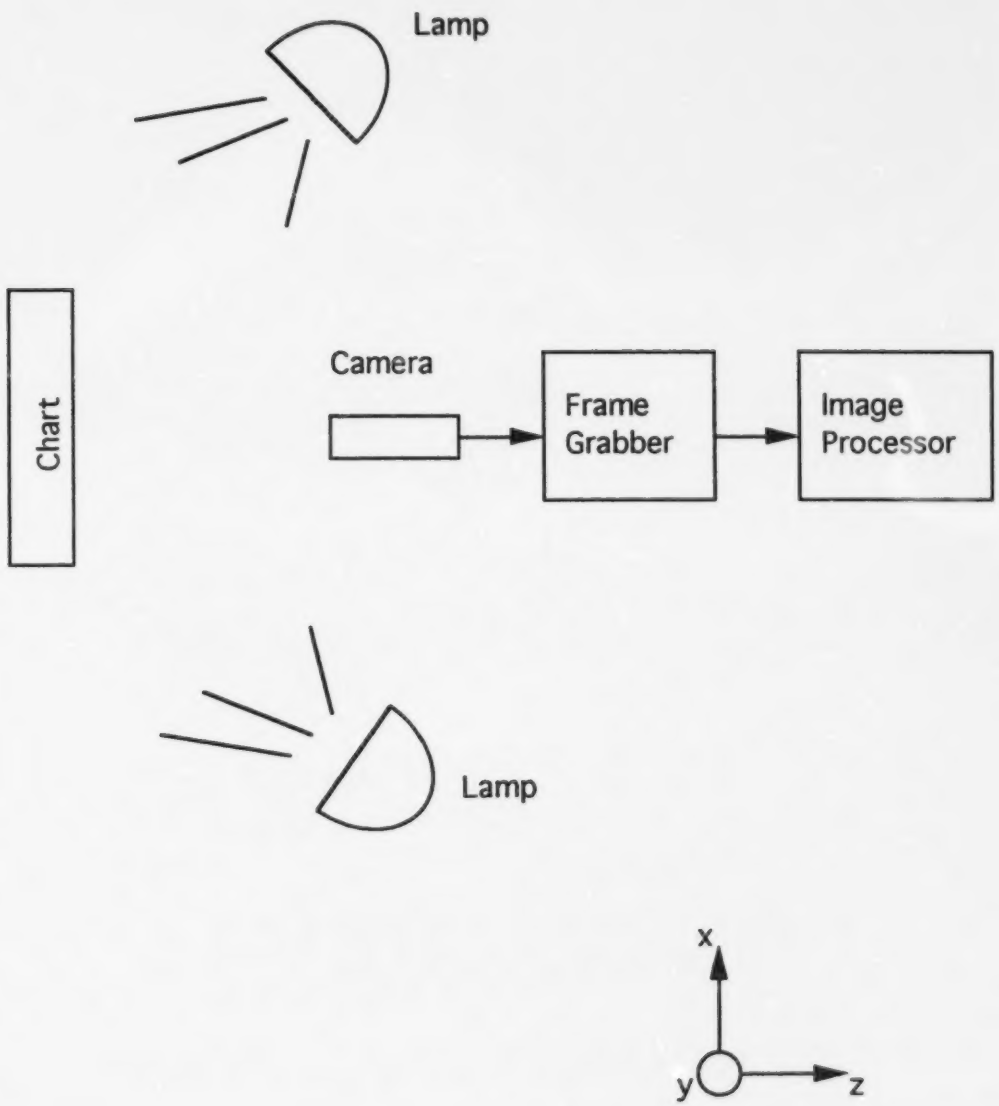

Figure 3.1: Layout for Determination of Overall Distortion and Resolution

A Computar 16 mm F/1.4 lens was compared to the Tamron SP 17 mm F/3.5 high performance ultra wide angle lens. All images were acquired using the same f-stop (4) and object distance (1.4 m) as used clinically.

To avoid perspective distortion which occurs when the object plane and the image sensor plane are not parallel, manual rectification was done using a camera mount which had 6 degrees of freedom. The two planes were considered parallel when points equidistant from the centre of the chart were imaged to have equal pixel distances from the centre of the image. An iterative translation/rotation procedure was used: x and y translation to align the centre of the chart with the centre of the image; x-axis rotation to establish equal vertical pixel distances; y-axis rotation to establish equal horizontal pixel distances; and z-axis rotation to ensure the centre horizontal line remained horizontal.

Special consideration was given to chart lighting, since this significantly affected the quality of the image data. Two studio lamps of 250 watts with spun glass diffusion covers and two reflector cards produced the best results. Contrast between black lines and white background was adequate with grey levels of approximately 180 for black and 130 for white (out of 256). Light intensity was consistent across the image (grey level = 130, range 115 to 145, for white) so there were no problems discerning control points in dark corners.

The chart was designed with a computer aided design graphics program and plotted on a high resolution 7570A HP plotter. It consisted of 21 vertical and 17 horizontal lines spaced 3.0 cm apart providing 357 control points for analysis. The chart was imaged and the control points digitized to obtain two dimensional pixel coordinates. Control points were compared to ideal coordinates to quantify overall image distortion. Ideal image points were computed by averaging distances between control points near the centre of the image and extrapolating the x and y distances across the entire image field. It was assumed that the centre of the image was distortion free since the lens centre exhibits significantly less distortion than the periphery (Horder, 1971).

Error vectors were produced showing the displacement of a point from an ideal position to its imaged position. The magnitude (to the closest pixel value) and direction of these vectors were calculated. Distortions were resolved into radial and tangential components.

To determine the effect of lens quality on distortion, the chart was imaged again using the F/3.5 lens and the distortions compared to those using the F/1.4 lens.

In all images, equivalent distances in object space appeared to be longer in the horizontal direction than they were in the vertical direction. This effect was also seen during the calibration procedure for these cameras (Peterson et al., in press). The

vertical to horizontal aspect ratio was determined by comparing vertical and horizontal dimensions of squares located at the centre and four corners of the field of view. This aspect ratio mismatch was eliminated from the data, and new error vectors calculated.

Repeatability and accuracy of the manual digitization procedure was investigated using a test/re-test procedure with 10 repetitions. The centroids of 20 light spots were digitized in 2 back surface images, one from the centre and the other from the left side. Digitization was done by the same user on five occasions over a one week period. The order in which the images were digitized was randomized. The centroids were visually estimated by the user and recorded by the image processing program. The image capture and processing programs had a resolution of one pixel. Since no sub-pixel analysis has been done, mean values were recorded to the nearest integer value and standard deviations were recorded to the nearest half pixel value.

Results and Discussion

Repeatability of point digitizing was ±1 pixel; the maximum error did not exceed 1 pixel.

Magnitude of the error vectors increased with distance from the centre of the image.

Since the error vectors are symmetrical, only the error vectors in the upper right quadrant of the image taken with the F/1.4 lens are shown in Figure 3.2. Control points near the centre were displaced by 0 or 1 pixels and those at the periphery were displaced by 5 pixels maximum (Table 3.1).

Table 3.1: Maximum Distortion in Pixels.

Lens	Maximum Error Magnitude	Maximum Radial Component	Maximum Tangential Component
F/1.4	5	5	2
F/3.5	2	2	1

The horizontal dimension of the imaged squares was 1.02 times the vertical dimension at all five locations across the field of view. Values in Table 3.1 indicate the distortion after this correction factor was incorporated.

After eliminating the aspect ratio mismatch, it was clear that the control points shifted towards the image centre. The magnification factor was less at the edges of the image than it was at the centre of the image. This type of shift is called barrel distortion (Mikhail, 1989). The maximum shift, after compensation for aspect ratio, was five pixels which corresponds to 5.4 mm in object space. A discrepancy of this magnitude in a topographic map of the back is quite serious. This distortion should

Upper Right Quadrant of Image

• = Imaged Location

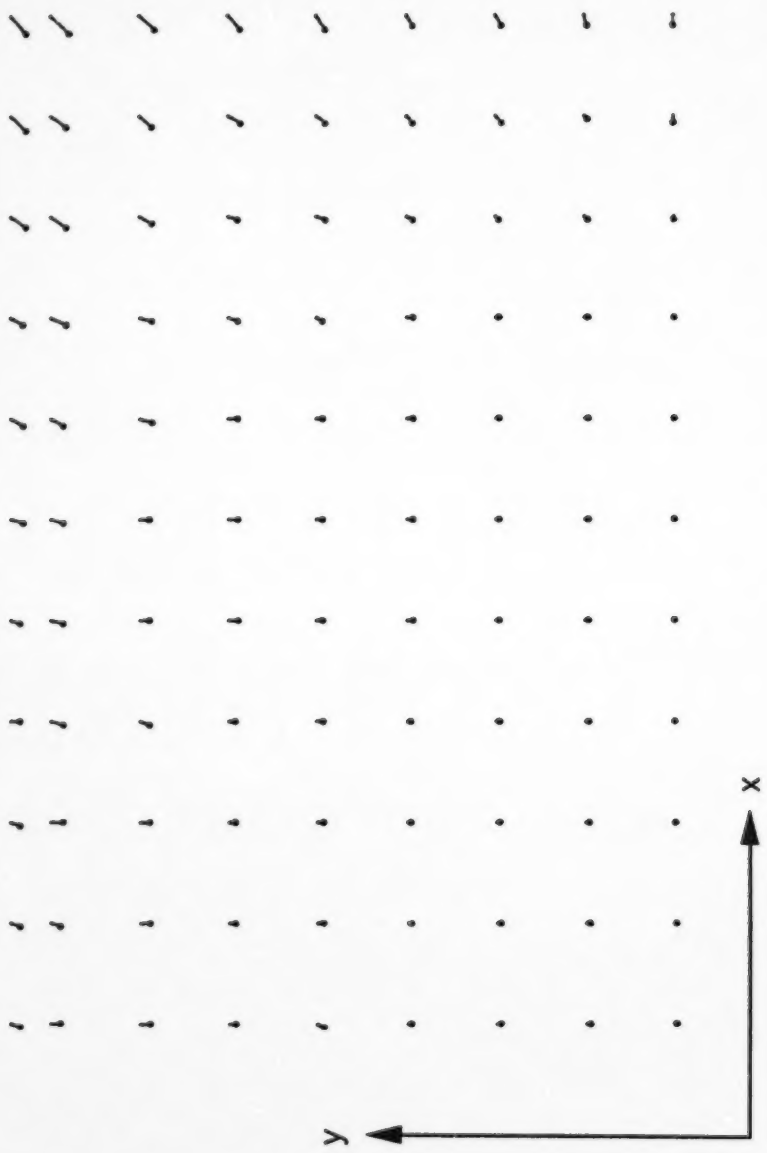

Figure 3.2: Error Vector Diagram

be corrected prior to using the data to map trunk deformities.

Image distortion was significantly affected by the lens used. A 3 pixel improvement on maximum distortion was observed with the F/3.5 lens. This corresponds to 3.2 mm distortion in object space.

3.2 Aspect Ratio

To examine the range of aspect ratios possible with the system the horizontal scanning frequency was adjusted with the Horizontal Automatic Frequency Control (H AFC). Images were captured at three frequency values: the lowest possible value obtainable (f=14.05 kHz), the value set by the manufacturers (f=15.75 Khz), the highest value obtainable before the camera and frame grabber lost synchronization (f=16.65 Khz).

The horizontal:vertical aspect ratio ranged from 1.14:1 to 0.96:1 by varying the H AFC (Figure 3.3). Mismatched aspect ratio of the image can be eliminated by adjusting the camera horizontal sampling rate (Wiesel & Voegtle, 1986). It is a simple electronic adjustment that simplifies the calibration routines at the image processing stage.

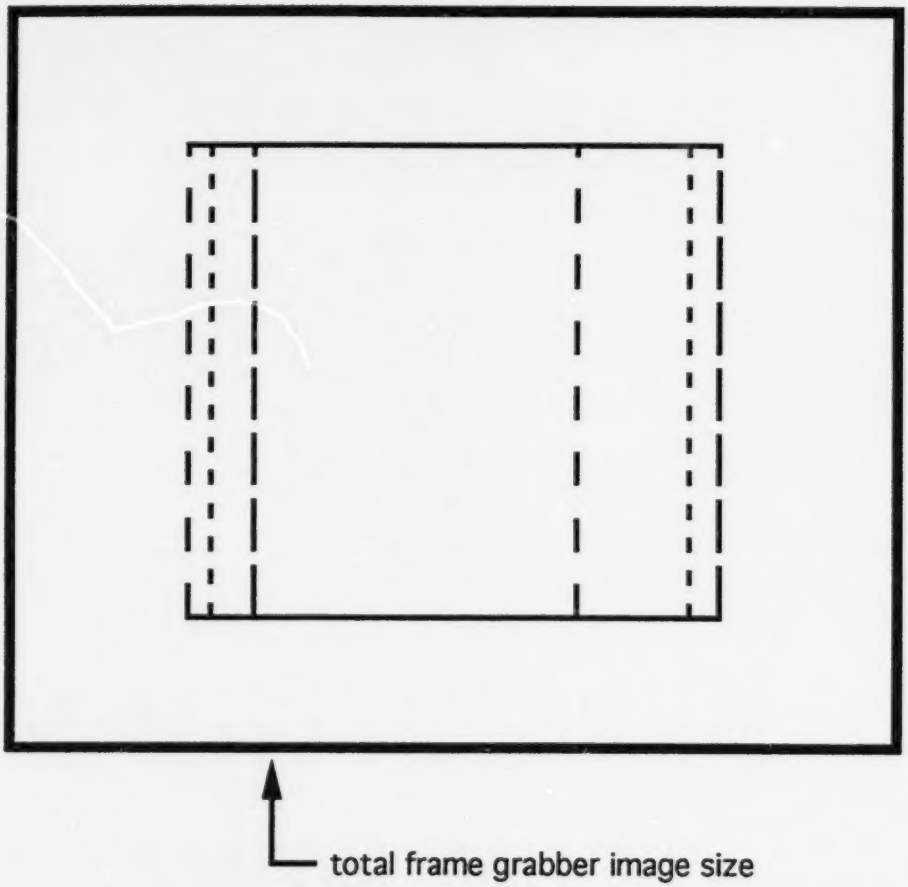
total frame grabber image size
Horizontal Scanning Frequency = 14.05 kHz
Horizontal Scanning Frequency = 15.75 kHz
Horizontal Scanning Frequency = 16.65 kHz

A square imaged by the frame grabber shifts across the captured image when the horizontal scanning frequency is adjusted.

Figure 3.3: Image Aspect Ratios

3.3 Overall System Resolution

Resolution describes how well two points in space can be discerned. Resolving power is expressed as the number of line pairs per millimetre (line pairs/mm) that can be distinctly resolved at the imaging surface. In this section overall system resolution is measured. Each stage of the video camera set up limits resolving power, and will be discussed in Chapter 5.

Materials and Methods

A chart with varying line pair distances was imaged to determine the point when lines could no longer be distinctly resolved. The layout for this experiment is shown in Figure 3.1. Charts consisted of line pairs which varied from 5 mm to 0.9 mm between line centres on a white background. Line pairs were oriented vertically to test the horizontal resolution of the camera. An F/1.4 lens was used. The images were captured at an f-stop of 4 and camera to image distance of 140 cm. Line pairs were imaged onto the centre of the camera lens, to minimize the effect of abberations present at the edge of the lens. The procedure to determine resolution described in the "IRE Standards on Video Techniques: Measurement of Resolution of Camera Systems" (1961) was followed.

Image and object planes were rectified as described in Section 3.1. Light intensity values at each of the four corners of the chart were measured with a light meter to ensure even lighting. The captured image was magnified in the image processing program and visually examined to determine when line pairs could not be resolved.

Results and Discussion

Line pairs became indiscernible at 2.3 mm between line centres in object space. To translate this value into image space the magnification factor, M, was calculated. In the distortion measurements from Section 3.1, 30 mm on the chart translated to 28 pixels on the frame grabbed image. The side of the sensor is 8.8 mm which maps onto 640 pixels. So:

$$M = \frac{size\ of\ im}{size\ of\ object}$$
$$= \frac{28\ pixels * \frac{8.8mm}{640\ pixels}}{30mm}$$
$$= 0.01283$$

and so the distance between maxima at the sensor surface is:

$$distance\ of\ maxima = 2.3mm * M = 0.0295mm$$

In one millimetre, thirty-four line pairs with 0.0295 mm between line centres can be resolved (34 line pairs/mm at the sensor surface).

CHAPTER FOUR: SENSOR CHARACTERISTICS

JVC TK-S310U cameras were not designed for high precision measurements so their performance is not accurately documented. The CCD sensors response to incident light was characterized by measuring its spectral response, linearity, sensitivity, bloom, and uniformity.

4.1 Background on Experimental Setup

This section describes common equipment used in the experiments to characterize CCD response to incident light.

Building Vibration

Suitability of the experiment site was investigated to determine if the optical set up should be isolated from building vibration. An accelerometer was used to measure the vibration at three locations around the laboratory, two on the counter top and one on the floor. The maximum vibration was 3 μm, measured on the counter top, and average vibration was 1 μm. The desired focal point diameter for the laser light

beam was 13.4 μm, the size of a CCD sensing element. Since average vibration was less than the desired accuracy no further isolation of equipment was necessary.

Light Source

Two types of lasers were used for light sources: a Helium Neon (HeNe) and a laser diode. In the linearity determination experiments the optical setup was aligned with the HeNe laser and then the laser diode was inserted to obtain sensor response measurements. In the remaining experiments only the HeNe laser was used. The laser diode produced light with wavelength 670 nm and the HeNe laser produced light with wavelength 633 nm.

To obtain a focal point size equivalent to sensor element pitch the Rayleigh principle was applied. The principle states that focal spot size will be smaller if the divergence of the beam, θ, can be reduced (Melles-Griot, 1988). The divergence of the beam is proportional to the inverse of the beam waist, w_0:

$$\theta \propto \frac{1}{w_0}$$

(Eq. 4.1)

Hence, the optical setup used in the following experiments allows the beam to diverge to increase w_0, then, extracts the centre portion of the beam where divergence will be minimum. This sampled beam is then focused to a very small

point size equivalent to sensor element pitch.

Laser Light Intensity Variation

It was necessary to vary the laser intensity across the dynamic range of the CCD. Several methods were considered: polarization filters, a prism reflection/re-aligning system, gelatin (gel) filters, and laser drive current variation. The method chosen was a combination of gel filters and laser drive current since these were inexpensive and readily available.

Several gel filters were calibrated to determine how much light they transmit at light wavelength of 670 nm. These filters were referred to as 4, 3, 1, 0.6, and 0.3, and they corresponded to 0.00032, 0.00098, 0.090, 0.225, and 0.48 transmittance of the original intensity. With these filters the full dynamic range of the CCD sensor could be investigated but not with enough resolution. To acquire the required resolution, a combination of gel filters and laser diode drive current variation was used.

The output light intensity of the laser diode can be varied from 0 to 100% of maximum by changing its input drive current. A current supply which provides the logarithm of the input voltage was built to control the laser diode light intensity (Figure 4.1).

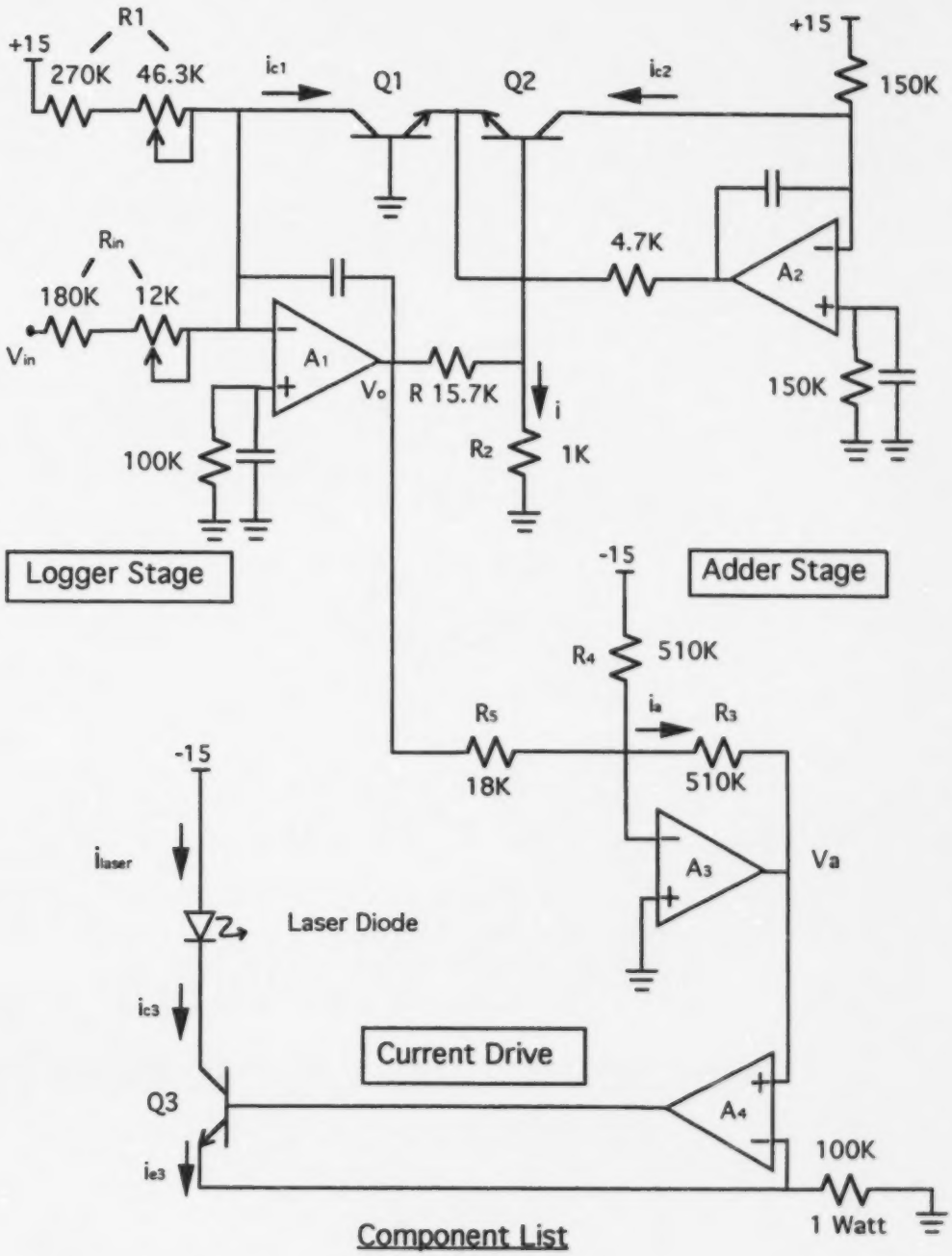

Figure 4.1: Logarithmic Current Drive Circuit Schematic

The circuit consists of three stages, the logger, the adder and the current supply. For the logarithm stage, the output of the logger stage, V_o, is the logarithm of the input voltage, V_i (Taub & Schilling, 1977; Jung, 1986):

$$i = \frac{V_{be_2} - V_{be_1}}{R_2}$$

(Eq. 4.2)

$$\begin{aligned} V_{be_2} - V_{be_1} &= V_T \ln \frac{i_{C_2}}{i_S} - V_T \ln \frac{i_{C_1}}{i_S} \\ &= V_T \ln \frac{i_{C_2}}{i_{C_1}} \end{aligned}$$

(Eq. 4.3)

$$\begin{aligned} V_o &= iR + V_{be_2} - V_{be_1} \\ &= V_T (\ln \frac{i_{C_2}}{i_{C_1}})(\frac{R}{R_2} + 1) \\ &= 26mV * 2.3 \log \frac{i_{C_2}}{i_{C_1}} (\frac{R}{R_2} + 1) \end{aligned}$$

(Eq. 4.4)

Assigning R_2 = 1 K and R = 15.7 K simplifies V_o:

$$V_o = \log \frac{i_{C_2}}{i_{C_1}}$$

$$\text{where } i_{C_2} = \text{constant}$$

$$i_{C_1} = \frac{V_i}{R_i} + \frac{15V}{R_1}$$

I_s, reverse saturation current, cancels in the above derivation, because, the two transistors are in the same IC package and should have identical characteristics.

The adder stage takes the low voltage signal from the logarithm stage, V_o, and translates it to a functional operating voltage, V_a, for the current supply stage:

$$V_a = -i_a R_3$$

$$i_a = \left(\frac{V_o}{R_5} - \frac{15V}{R_4}\right)$$

$$V_a = 15 - 28.3 V_o$$

(Eq. 4.5)

Current is supplied through transistor Q_3 and is limited with the 1 Watt 100 Ω resistor:

$$i_{laser} = i_{c_3} \cong i_{e_3} = \frac{V_a}{100}$$

(Eq. 4.6)

The logarithmic current supply was calibrated to determine the current levels

corresponding to desired laser output light intensities. The current input which generated the maximum laser light intensity, termed 100% intensity, was established. The current values required to attain power intensities at 10% intervals down to 0% were determined.

Current supply calibration done on different days yielded very different output intensities. This was attributed to the power intensity meter; the meter's output was very sensitive to the location of the input beam. Because of this day to day variation, calibration of the logarithmic current controller was performed before each set of experiments.

4.2 Spectral Response

Spectral response was measured to determine what wavelength the sensor was most responsive to. A spectrophotometer was used as a light source for wavelengths from ultraviolet to infrared. The lens was removed from the camera, so values reflect sensor response only. There was a protective glass cover over the CCD sensor which may have influenced the spectral response slightly.

The output video signal magnitude at incident light wavelengths from 350 to 1100 nm is indicated in Figure 4.2. As predicted by Eq. 2.2, sensor response stops at cut-off

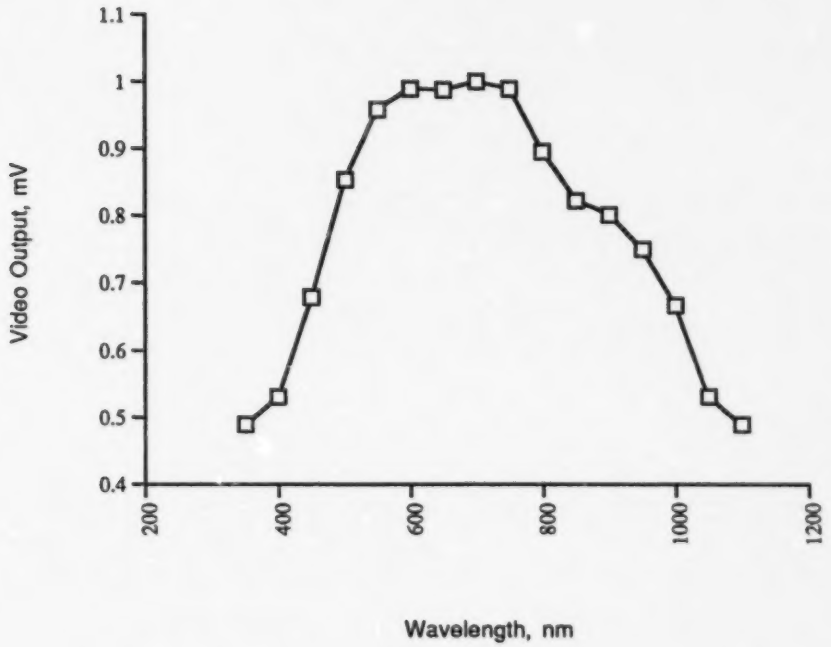

Figure 4.2: Spectral Response of Image Sensor

wavelength 1100 nm. Clearly, the camera responds better to red and infra-red light than lower wavelength visible light.

4.3 Linearity

The purpose of this experiment was to determine if the voltage output from the CCD sensing elements was linearly proportional to incident light. The laser light source was focused onto the sensor, its intensity varied, and the output of the CCD sensor was recorded.

Materials

The laser diode light source was varied with the logarithmic current supply and gel filters. The laser beam was focused through the combination of the iris, diverging lens, and microscope objective onto the CCD sensor (Figure 4.3).

The laser light beam diverges slightly as it travels through the first 4.2 cm, then, only the central 1 mm of the beam passes through the iris. That beam diverges as it travels 10.3 cm to the diverging lens where it diverges even more. Only the central part of the beam passes through the iris of the microscope objective (Cooke 10 x .25 A3579). The microscope objective lenses focus the beam onto the CCD sensor

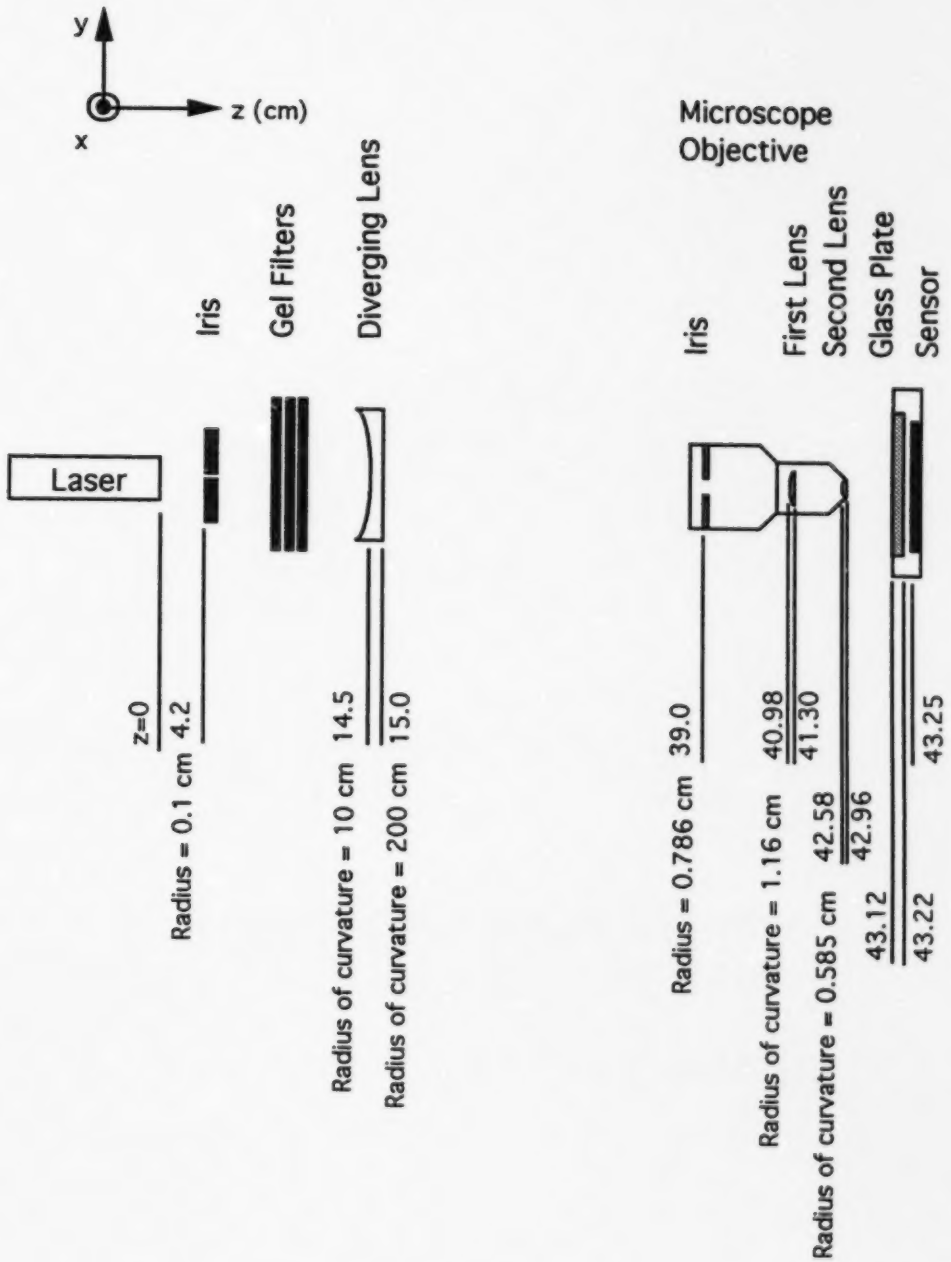

Figure 4.3: Optical Setup for Linearity Determination

through a plate of glass, approximately 0.75 mm thick, mounted on the IC package. This glass protects the sensor from dust and damage, however, it also causes some diffraction of the beam.

The reason for allowing the beam to diverge, and then, sampling only the central portion of it is because the centre has a gaussian distribution with low divergence and low noise.

The diameter, diam, of the focal point with a simple lens can be determined, theoretically, by (Winburn, 1987):

$$diam \approx f\theta \qquad \text{(Eq. 4.7)}$$

where, f = focal length and θ = beam divergence. When a beam has travelled to the far field the focal point diameter d_{diff}, diffraction limited diameter, is given by:

$$\begin{aligned} d_{diff} &= 2.44\frac{f\lambda}{d} \\ &= \frac{2.44 * 3mm * 670nm}{1mm} \\ &= 4.9\mu m \end{aligned} \qquad \text{(Eq. 4.8)}$$

where, d = diameter of the beam.

The focal point size of the laser beam at the CCD sensor using this optical setup was

calculated using an optical ray tracer program, "Beam 2" (Beam 2: Optical Ray Tracer, 1986). The mathematical foundation used by the ray tracer program was developed by Spencer and Murty (1962). The program requires measurements for distance along z axis, radius of curvature, shape of curvature, and type of surface.

Distance between lenses and radii of curvature for the microscope objective were measured on a similar objective, Cooke 10 x .25 A7045. The surface topography of each lens was measured with a profilometer and the radius of curvature calculated from that data. The radius was 11.6 mm for the first lens and 5.85 mm for the second lens.

Using these parameters "Beam 2" predicted that the focal point size at the CCD surface was 18 μm. Sensing elements on the CCD sensor are 13.6 μm by 13.4 μm, thus, the sensing element was completely covered with light. This ensured full response from the sensing element.

Methods

The optics were aligned using the HeNe laser light source. The logarithmic current supply was calibrated, then the HeNe was replaced by the laser diode, and the laser diode was aligned with the succeeding optics.

The dynamic light range of the CCD sensor was determined. The gel filters required to attenuate the laser light intensity to a level slightly higher than that which saturates the CCD sensing elements were 3, 3, and 0.3 together. The filters required to attenuate the laser light intensity to a level slightly higher than that which the CCD sensor will no longer detect were 4, 3, and 0.6 together. The following combinations were used to span the entire dynamic range: (3, 3, 0.3), (3, 3, 0.6), (4, 3), (4, 3, 0.3), (4, 3, 0.6). Each step represents approximately a 1/2 intensity reduction.

The beam was focused onto one CCD sensing element using the camera mount adjustments. The z axis was adjusted until the smallest spot size was produced. Then sensor tilt around the z axis was adjusted to make the x axis horizontal. The camera mount was translated in x and y to obtain maximal sensing element signal response. Then tilt around the x and y axes were adjusted until there was equal spill over onto adjacent pixels. All of these adjustments were observed on the oscilloscope. The current was ramped from 100% down to 60% for each filter combination. Sensor output voltage and video signal voltage of the target sensing element were measured at each intensity increment.

Results

The output voltage of the target CCD sensing element at each input light intensity

variation is shown in Figure 4.4. Although the CCD sensor was responsive to light intensities over a larger range, the range of light intensity indicated is that which the frame grabber could respond to. The best line of fit for the data had an $r^2 = 0.975$. After the linear sensing element response undergoes the signal processing stage, the response is no longer linear (Figure 4.5). Chapter 5 discusses the implications of a non-linear response.

4.4 Saturation Voltage

Sensor response to light saturates at a point called the saturation voltage. Saturation voltage for this CCD sensor was 71.88 mV. Any voltages greater than this will not be indicative of the actual quantity of light incident upon the sensor.

4.5 Quantization

The charge packet which gathers at an electrode of the CCD is proportional to the incident light in that region. Quantization is an expression which relates the change in CCD sensor output voltage to a change in input light intensity.

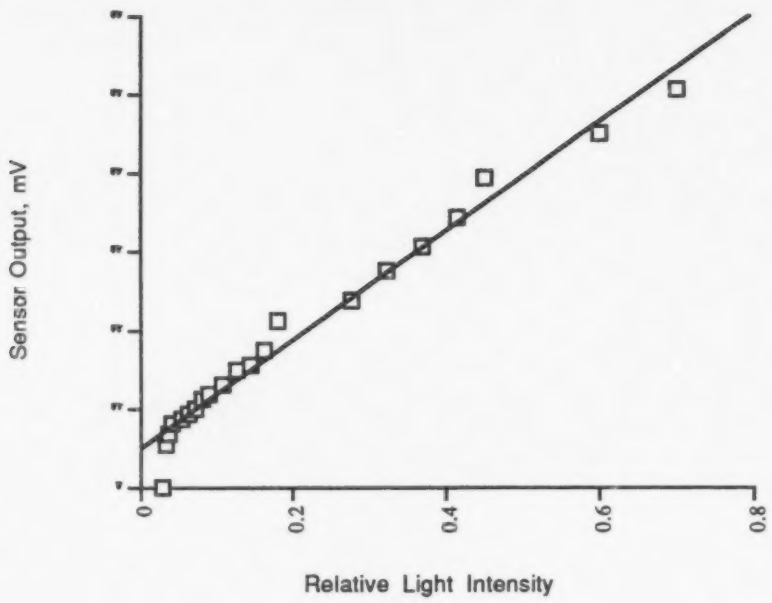

Line of Best Fit $= 69.301x + 4.953$ $r^2 = 0.975$

Figure 4.4: CCD Sensor Response for Linearity Determination

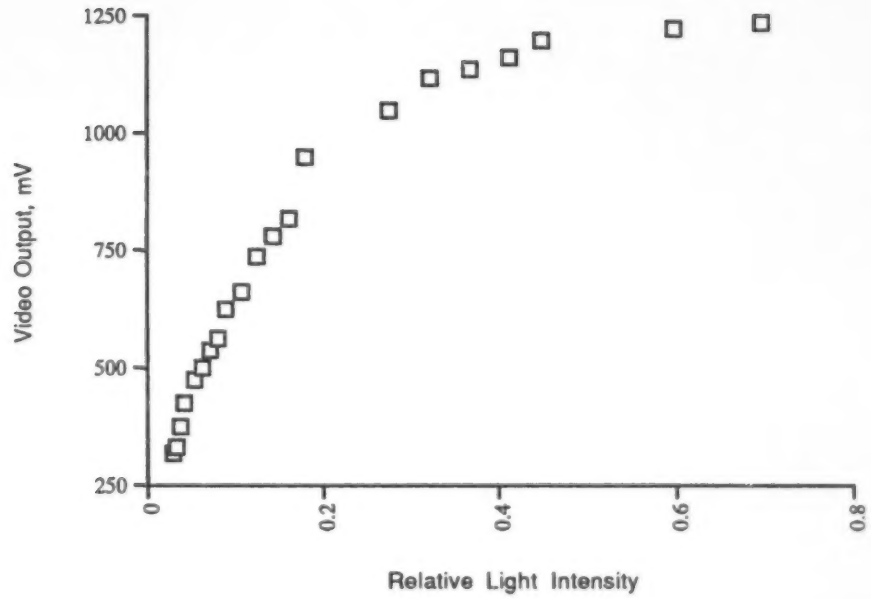

Figure 4.5: Video Signal Response for Linearity Determination

The intensity of the full beam of the laser diode was 0.72 mW. The part of the beam which passed through the iris contained 20 μW of that intensity:

$$0.72mW * \frac{\pi r_{iris}^2}{\pi r_{all}^2} = 0.72mW * \frac{\pi 1mm^2}{\pi 6mm^2} = 20\mu W$$

This intensity was attenuated by 4 gel filters (a 4, 3, and 0.3) and by four glass interfaces (diverging lens, 2 microscope objective lenses, and protective glass on sensor IC), to 4 x 10^{-12} W. When this intensity was decreased by half the sensor signal changed by 9.37 mV, the video output changed by 325 mV and the pixel grey value on the frame grabber changed by 86. Thus, quantization is 213 x 10^{-12} W/V for the sensor, 6.15 x 10^{-12} W/V for the video signal and 0.02 x 10^{-12} W/grey level for the frame grabber.

Each grey level of the frame grabber represents approximately 0.11 mV change at the image sensor output (ie. 9.37 mV/86 grey levels = 0.11 mV/grey level). This value is approximate because the relationship between light intensity and frame grabber output is not linear.

4.6 Bloom

The purpose of this experiment was to quantify how much charge is detected at its neighbours when a sensing element is over exposed. This was determined by increasing the magnitude of light incident upon one sensing element past saturation and observing the response of surrounding pixels.

Materials

The HeNe laser was used as the light source. Light intensity was varied using gel filters and glass slides. A diverging lens, iris, and microscope objective were used to focus the laser beam onto the CCD sensor (Figure 4.6). An average of eight frames of the video signal was taken with the "Image" image capture program. The sensor signal was measured at the output of the CCD sensor IC. Shielding was placed around the camera circuit boards.

Glass slides were used to attenuate the laser light to obtain intermediate intensities between gel filters. Combinations of two glass slides were calibrated to determine their filter strength at light wavelength of 630 nm.

The laser light beam diverges as it travels through the first 239.5 cm, the diverging

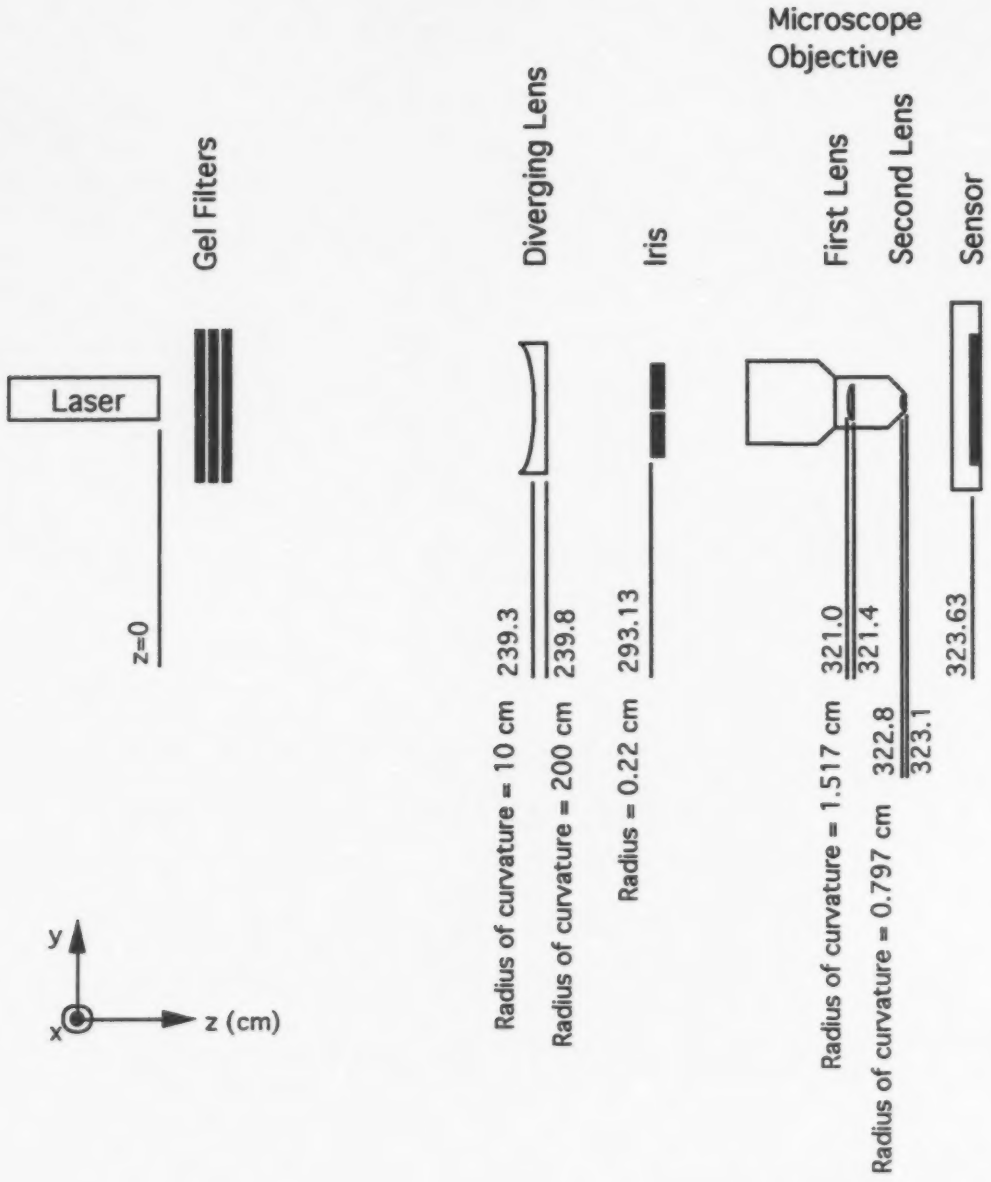

Figure 4.6: Optical Setup for Bloom Determination

lens and the next 54.1 cm. At the iris, only the central 2.2 mm diameter of the beam goes on. That beam is focused by the microscope objective (Reichart 10/0.25) onto the CCD sensor. Parameters for the microscope objective required by the ray tracer were calculated from profilometer measurements of the surface profile of the lenses. The protective plate of glass on the CCD package was removed and the ray tracing program, "BEAM 2", calculated the focal point size on the CCD sensor to be 12 μm. The size of the sensing elements is 13.6 μm x 13.4 μm, thus, there was no optical spill over of light to neighbouring sensing elements.

Methods

The optical system was aligned. The beam was focused onto one CCD sensing element using the camera mount adjustments. These adjustments were observed on an oscilloscope.

Gel filters required to attenuate the laser light to the range around which the CCD sensor would saturate were determined. The gel filters required to attenuate the laser light intensity to a level slightly lower than CCD sensor saturation were 3, 3, and 0.3. The filters required for a level slightly higher than saturation were 3, 3, 0.6, and 0.3. The following filter combinations were used to span the entire range: (3, 3, 0.3), (3, 3, 0.6), (3, 3, 0.6, 0.3). Each step represents approximately 1/2 intensity reduction.

Intensity was varied across the range of interest using each combination of gel filters and glass slides. Sensor voltage and video signal voltage for the target sensing element and the top, bottom, left and right neighbours were recorded. In addition, an eight frame average frame grabber image was captured at each intensity level.

Results and Discussion

Saturation voltage for the target sensing element occurs at 71.88 mV which corresponded to 0.4 normalized intensity. Figure 4.7 shows that this is when neighbouring sensing elements begin to show an increased output. This increase indicates spill over of charge from the target pixel. The amount of charge spill over is significant, particularly for the right neighbour. The voltage spill over to the right neighbour was 16.25 mV, and to the other neighbours, 4.1 mV. In terms of saturation voltage (71.88 mV), the right neighbour received 16.25 mV/ 71.88 mV * 100% = 23% spill over and the other neighbours received 4.1 mV/ 71.88 mV * 100% = 6% spill over. Since a change of 0.11 mV at the sensor output generates one grey level change on the frame grabbed image, 16.25 mV spill over implies the right neighbour's grey level will be in error by 147. Since there are only 256 grey levels in total, 147 is a very significant error.

The video signal does not indicate this spill over as clearly (Figure 4.8). Intensity

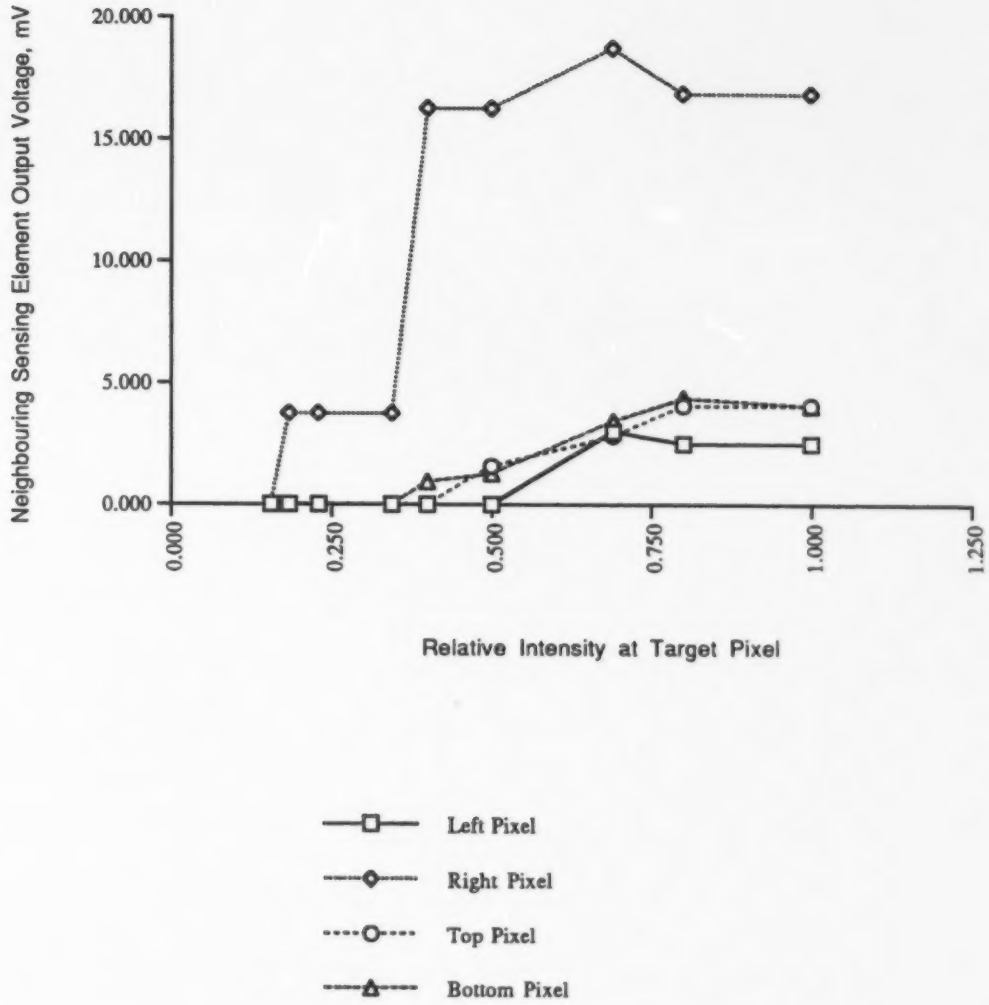

Figure 4.7: Sensing Element Response for Bloom Determination

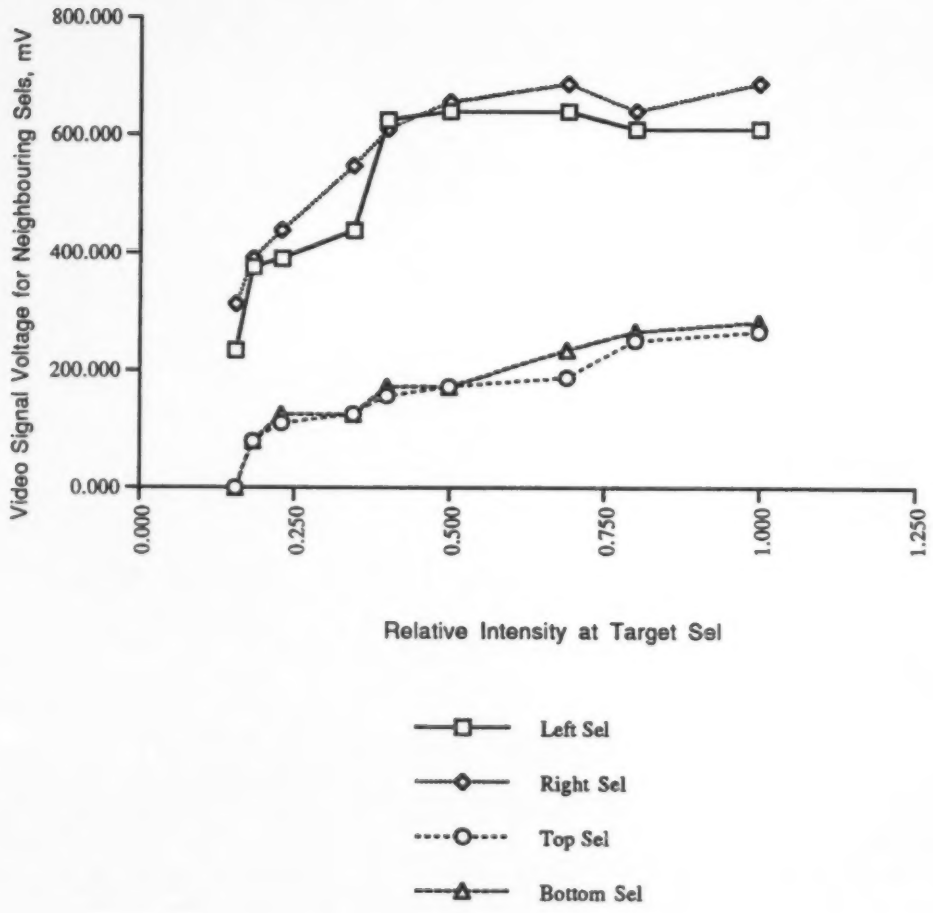

Figure 4.8: Video Signal Response for Bloom Determination

information for one sensing element is spread over a range of approximately five sensing elements because of camera signal processing. Hence, voltage representing spill over is obscured by this spreading of the signal. Chapter 5 evaluates and discusses the implications of bloom on overall system distortion and resolution.

Initially, this experiment was attempted with the laser diode, however, the laser beam could not be focused onto one sensing element. This is probably due to poor laser lens quality and high order transverse electromagnetic (TEM) modes. TEM_{lm} modes occur in the plane perpendicular to the axis of the optical cavity. The subscripts l and m indicate the number of times the electromagnetic field crosses the x and y axes respectively. TEM_{00} has a gaussian distribution, whereas higher order modes produce beam profiles with bright and dark patches. It is desirable to emit only TEM_{00} because it has minimum divergence, minimum diffraction loss, and can most easily focus down to a diffraction-limited spot size (Winburn, 1987; Melles-Griot, 1988). The phase changes in the higher order modes of the laser diode limited the minimum spot size attainable.

4.7 Uniformity

The purpose of this experiment was to examine the repeatability of sensing element output as a function of sensing element location. The same laser and optical set up

as used in the bloom determination experiments was used for this experiment (Figure 4.6).

The beam was focused onto the CCD sensor. The CCD sensor was made perpendicular to the laser light beam using the camera mount adjustments. It was required that the distance from the microscope objective to sensor surface remain constant so the intensity and focal point size of the light at all sensing elements were consistent.

The camera mount adjustments were used to translate the CCD sensor so the laser beam focused on eight positions around the sensor, four near the centre, and one near each corner. CCD sensor output was measured at two levels of intensity at each location, one near sensor saturation and the other at mid-range.

Results

Images of the light spots indicated that the spot diameter was greater at the corners than at the centre. Thus, data for the four corner samples was eliminated because the light intensity was not uniform. At medium light intensity, mean sensor output voltage was 13.6 mV, with a standard deviation of 2 mV (15%) and a range of 11 to 16 mV (sample size = 4). At high light intensity, mean sensor output voltage was 71.4 mV, with standard deviation of 8 mV (12%) and a range of 60 to 78 mV (n=4).

The uniformity of incident light intensity is very sensitive to distance from lens to sensor. This may explain why these results do not support the findings of other investigations which indicate that uniformity decreases as light intensity increases (Little, 1977).

4.8 Summary

Sensor response characteristics which were determined in the previous sections are summarized as follows:

Table 4.1: Summary of Sensor Characteristics

Linearity	$r^2 = 0.975$
Quantization	213×10^{-12} W/V
Bloom	23% (Right Neighbour) 6% (Others)
Uniformity	12% (High Intensity) 15% (Low Intensity)

CHAPTER FIVE: INDIVIDUAL ERRORS

In this section, individual contributions at each stage of the image capture system are quantified to determine their effect on overall system resolution and distortion. Concentration is on the lens and the CCD sensor. As shown in Chapter 3, overall maximum distortion was 8.6 mm and overall system resolution was 34 line pairs/mm.

5.1 Lens

Distortion, diffraction and chromatic abberation for this surface topography measurement system were investigated. The distortion exhibited by the F/1.4 and F/3.5 lenses is barrel distortion. The F/1.4 lens caused point localization errors of up to 5.4 mm (Chapter 3). Distortion decreased by 3 pixels when using the F/3.5; so the amount of overall distortion attributable to the F/1.4 lens is 3.2 mm in object space. This is a significant systematic error which may be corrected at the image processing stage. Radial and tangential correction factors can be applied to each data point of the captured image.

Stopping down, ie. making the aperture smaller, is a technique used to decrease lens abberation effects which are typically more apparent at the lens periphery. However,

this causes more diffraction of the light rays. The limit on resolvable line pairs resulting from this diffraction can be determined. Lines will appear distinctly resolved if the separation between their centres is equal to approximately 1/2 of the Airy disk defined by diffraction theory. The Airy disk for the lens used in the surface topography measurement system is:

$$\begin{aligned} Airy\ disk &= 2.44\lambda N \\ &= 2.44 * 670nm * 4 \\ &= 0.0065mm \end{aligned}$$

(Eq. 5.1)

where, N = f-number. In object space this implies a 0.5 mm disk of uncertainty of placement.

The spectral distribution of the illumination light used in imaging applications must be considered when evaluating point accuracy (Hakkarainen, 1986). Because of chromatic abberation, a point source of white light, a combination of all visible wavelengths, cannot be imaged to a single point.

The index of refraction in crown glass for visible light ranges from 1.520 to 1.534 (Melles-Griot, 1988). An optical ray tracing program was used to examine variation in focal spot size when the index of refraction varies across this range (BEAM 2: Optical Ray Tracer). The focal spot size varied by 20 μm using a simple planoconvex lens with a focal distance of 16 mm. Thus, a point source of white light can potentially de-focus to a diameter of 20 μm on the sensor surface. Since de-focusing

is symmetric, the centroid of a light spot can still be accurately located, however, the resolving power of the lens is still limited. The light used in the surface topography measurement system is white and, unless this source is changed, the defocussing error cannot be eliminated. In this measurement system 20 μm corresponds to 1.5 mm in object space. However, the lens likely has chromatic abberation correction built into it, so the amount of de-focusing will not be this large.

Illumination at the imaging surface decreases proportionally to $\cos^4\theta$, where θ is the angle the portion of the image field in consideration makes with the lens axis (Welford, 1991; Horder, 1971; Little, 1977). This is due to the nature of light and is not a lens defect. This effect was obvious when obtaining distortion images in Chapter 3 and in back surface images. The diagonal distance of the imaging surface on the CCD is $(8.8^2 + 6.6^2)^{1/2} = 11$ mm. The focal length of the lens is 16 mm. Based on these values, $\theta = 37.5^\circ$ (Horder, 1971). Thus, $\cos^4\theta = 0.4$ and there will be a fall off to 40% intensity at the corners of the field. To give the imaged output uniform intensity, the object must have extra illumination at the edges. Although a scaling factor can be applied to the data at the periphery, some detail may be lost.

Patient backs in the surface topography measurement system spans across a region which may extend beyond the depth of field of focus for the lens. A basic photography rule is to focus one third of the distance between the closest and

farthest points. For example, if the back ranges from 130 to 160 cm from the camera then the focal distance should be set at 130 + 10 cm = 140 cm. This estimation is based on the following relation. Hyperfocal distance, h, is the distance from the lens to the nearest object which is just acceptably sharp when the lens is focused at infinity. It is defined by:

$$h = \frac{f^2}{cN}$$

(Eq. 5.2)

In the case of the GRH surface topography system, N = f-number = 4 and f = focal distance = 16 mm. C, circle of confusion, is equal to 1/(1/2(minimum resolvable lines/mm on sensor)). Minimum resolvable lines/mm on the sensor = 36.8 lines/mm (Section 5.2), thus, C = 0.0545 mm. The hyperfocal distance, h, equals 1.2 m. When the lens is focused at a finite value, u, the distance, x, from the lens to the nearest point in acceptably sharp focus equals (h * u)/(h + u). The distance, y, from the lens to the farthest point in acceptably sharp focus equals (h * u)/(h - u). The distance the lens should be focused on is found by solving these equations for u. For the case of the Glenrose, with x = 130, and y = 160, u = 2xy/(x + y) = 143 cm.

In practice, using these guidelines produces an image that is not sharp due to lens abberations and the behaviour of light waves. Indeed, light spots on the sides of the back in the images from the GRH system indicate significant defocussing.

5.2 Sensor Geometry

The pitch of the sensing element was calculated to determine the maximum resolving power of the CCD sensor.

Given that:

NH = number of horizontal sensing elements = 649

NV = number of vertical sensing elements = 491

H = horizontal sensor size = 8.8 mm

V = vertical sensor size = 6.6 mm

The size of a sensing element is:

$$s_x = \frac{H}{NH} = \frac{8.8mm}{649} = 13.6\mu m$$
$$s_y = \frac{V}{NV} = \frac{6.6mm}{491} = 13.4\mu m$$

(Eq. 5.3)

Given these sensor dimensions, the resolving power in the horizontal direction is 36.8 line pairs/mm and in the vertical direction, 37.3 line pairs/mm.

The consistency of sensor placement has been defined as 0.2 pixel pitch (Mori & Hirokane, 1989). Relative sensor spacing due to temperature changes is negligible, 0.03% ± 0.04% (Reimar and Fritsch, 1990). SiO_2 or metal layers may vary in

thickness, however, the thickness of these depositions is much less than the total surface area of the sensor. Based on these facts, sensing elements were assumed to be precisely located in x and y directions in one plane.

The Modulation Transfer Function, MTF, discussed in Chapter 2, falls at higher frequencies due to the limit that size and pitch of the sensors place on the sensor resolution capabilities. This is called the Geometric MTF (Beynon & Lamb, 1980; McCaughan & Holeman, 1979). It is calculated from the Fourier transform of the basic cell (Beynon & Lamb, 1980):

$$MTF_{geom} = \frac{\sin(\frac{s}{\pi g l})}{\frac{s}{\pi g l}}$$

(Eq. 5.4)

where, s = sensor pitch, g = normalized spatial frequency, and I = the sensitive region.

The light sensitive regions of the pixel pitch, s_x and s_y, are I_x and I_y. The output response from a particular sensing element occurs at the same time regardless of where it was illuminated within I_x. Thus, the output impulse will vary spatially with respect to the input illumination source position. If there is no optical band limiting before spatial sampling then the error in locating the illumination source is $\pm I_x/2$ and $\pm I_y/2$ (Lenz & Fritsch, 1990). For the GRH system, these values correspond to

location errors of (13.6μm/2) = 6.8 μm and (13.4 μm/2) = 6.7 μm (0.5 mm in object space). Locating the illumination source will be impossible if illumination lands on the blind region of size (s_x - I_x) or (s_y - I_y) since there will be no output at all.

Subpixel approximation techniques can be used to make the system space-invariant and decrease this location error. The shift of an input step function relative to the centre of the light sensitive area is transformed into the output amplitude, A(s), (Lenz and Fritsch, 1990). If this relationship between A(s) and shift from centre is known, grey level interpolation can be used to determine the exact location of the illumination source. Thus, the system becomes space-invariant.

Regardless of how well the edge of the sensor can be defined physically, there will be error defining sensor element edge due to its sensitivity distribution. There is a gradual transition from sensitive to blind regions. Definition of the sensitivity distribution profile gives more accurate spatial integration area measurements for use in the precise evaluation of resolution (Ohnishi & Murakami, 1985).

When an image is projected onto a CCD sensor, the continuous image is transformed into discrete space (Figure 5.1). Errors generated because of this transformation are called digitization errors. Errors due to discrete image representation have been developed using statistical techniques (Chih-Shing, 1983; Havelock, 1989; Lenz and Fritsch, 1990). Chih-Shing (1983) estimated the positional error in terms of the

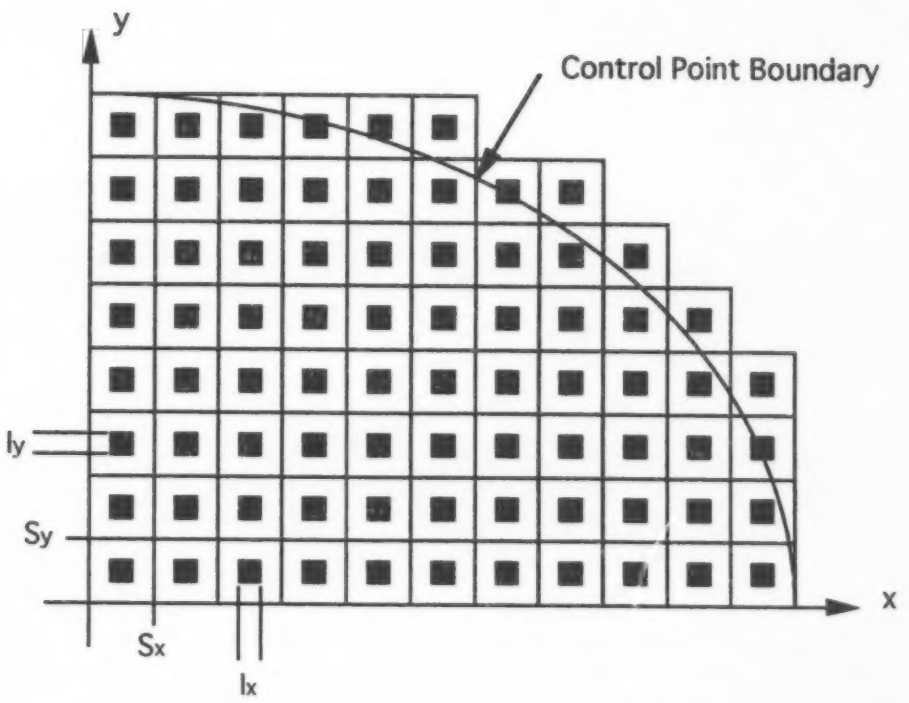

S_x, S_y = Sensing element pitch
l_x, l_y = Sensitive region of sensing element

Figure 5.1: Continuous Image Transformed into Discrete Space

dimensionless perimeter of an object. If the spatial frequency of the sensing elements is increased, the digitization error can be reduced. Chih-Shing's technique measures spatial quantization errors; however, intensity quantization also limits precision (Havelock, 1989). Havelock developed a model for analysis of position uncertainty which can be applied to general grey scale shapes. Havelock's model indicates that the number of quantization levels per pixel is more important than pixel size in determining precision.

The surface topography system image processing stage calculates centroid coordinates of the light spot images. The variance on the centroid coordinate can be determined. Given that errors are evenly distributed between $\pm 0.5\ s_x$, the mean square boundary location error, σ_b^2, is (Lens & Fritsch, 1990; Chih-shing, 1983):

$$\sigma_b^2 = \frac{\int_{\frac{-s_x}{2}}^{\frac{s_x}{2}} x^2 \delta x}{\int_{\frac{-s_x}{2}}^{\frac{s_x}{2}} \delta x}$$

$$= \frac{s_x^2}{12}$$

$$\sigma_b = 0.289 s_x$$

(Eq. 5.5)

The contribution of the error of one boundary to the error of the x coordinate centre estimate, $\sigma^2_{c(one)}$, is found by calculating the first order moment in x divided by the

total area of the ellipse:

$$\sigma^2_{c(one)} = \left(\frac{x\sigma_b s_y}{\pi r_x r_y}\right)^2$$

$$= x^2\left(\frac{\sigma_b}{\pi r_x n_y}\right)^2$$

where $n_y = \frac{r_y}{s_y}$, r_y = *radius along y* , r_x = *radius along x*

(Eq. 5.6)

It follows that:

$$\sigma^2_{c(ave)} = x^2_{ave}\left(\frac{\sigma_b}{\pi r_x n_y}\right)^2$$

x^2_{ave} is calculated:

$$x^2_{ave} = \frac{\int_0^{r_y} (r_x^2 - y^2(\frac{r_x}{r_y})^2)\delta y}{\int_0^{r_y} \delta y}$$

$$= \frac{r_x^2 y\Big|_0^{r_y} - \frac{1}{3}(\frac{r_x}{r_y})^2 y^3\Big|_0^{r_y}}{y\Big|_0^{r_y}}$$

$$= r_x^2 - \frac{1}{3}r_x^2 = \frac{2}{3}r_x^2$$

(Eq. 5.7)

Four n_y boundary elements with the average x^2 coordinate, $x_{ave}{}^2$, contribute to $\sigma_c{}^2$. If P and Q are independent variables, then, VAR(P+Q) = VAR(P) + VAR(Q),

hence, the variances $\sigma_{c(ave)}^2$ can be added to get total variance on the centroid coordinate, σ^2_c:

$$\sigma_c^2 = 4n_y\sigma_{c(ave)}^2$$

$$\sigma_c^2 = 4n_y\frac{2}{3}r_x^2\left(\frac{\sigma_b}{\pi r_x n_y}\right)^2$$

$$= \frac{8}{3n_y}\left(\frac{\sigma_b}{\pi}\right)^2$$

$$if\ \sigma_b^2 = \left(\frac{s_x}{12}\right)^2$$

$$\sigma_c = \sqrt{\frac{8}{3}}\frac{1}{\sqrt{n_y}}\frac{s_x}{\sqrt{2}\pi}$$

$$= 0.15\frac{s_x}{\sqrt{n_y}}$$

(Eq. 5.8)

So, the RMS error in the x direction is inversely proportional to the square root of n_y in the y direction. In this surface topography system, $n_x = 3$ and $n_y = 2$. Thus, the error of the x coordinate estimate, σ_c, is 1.44 μm (0.1 mm in object space). The error of the y coordinate estimate, σ^2, is 1.16 μm (0.09 mm in object space). This relationship shows that the variance on centroid coordinates can be reduced by decreasing the sensor pitch, or, increasing the control point size.

Just as in sampled electrical signals, sampled images form replicas (harmonics) of the power spectrum in the spatial frequency domain. These replicas can overlap with the actual image spectrum. The amount of overlap depends on the sampling rate and the actual image spectrum. If the actual image spectrum has low spatial frequency

content there is less chance for overlap. However, if the actual image spectrum has high spatial frequency, like, hard edges or regular repetitive patterns (like the regular dot pattern used in the back surface measurement system) there is a greater risk for aliasing. At a constant pitch, the amount of aliasing increases as the pixel size decreases (Kriss, 1990). Anti-aliasing can be performed by inserting an optical low-pass filter between the lens and image sensor (Kazunori & Murakami, 1985); or, by shifting the image by a fraction of the pixel pitch using a birefringent filter (Kriss, 1990). The most effective shift is approximately 0.5 x pixel pitch. This shift presents information to a sensing element that was originally imaged onto the inter element spacing.

5.3 Sensor Characteristics

The sensor characteristics measured in Chapter 4 can also limit overall resolution and distort imaged points.

Spectral Response

The semiconductor material on which the CCD is fabricated is more sensitive to light of red and infrared wavelengths than it is to the light at the low end of the visual

spectrum. Thus, imaged grey levels representing different colours of a scene will not accurately interpret illumination intensity with respect to each other. Since the surface topography images are currently done with white light this is not a concern. However, it is important to get the widest dynamic range of output from the sensor. This can be accomplished by using red or infra-red light for the light spot pattern which is projected onto the back surface. Red light may be more comfortable for the operator to use since it is visible. Another factor which insures the widest dynamic range of the system is that skin reflects red light more efficiently than the other visual light wavelengths (Regan & Parrish, 1982).

Linearity

CCD sensors are widely used because they are cited to have a very linear response to light intensity. Sensor manufacturers generally express linearity as less than 1% (EG&G, 1989). Indeed, some investigators have found deviation from a linear response of less than 0.1% (Epperson, 1987). A best line fit was approximated to the output signal from this CCD sensor yielding an r^2 of 0.975 (Figure 4.4).

The image processing stage of a surface topography system detects light spot edges and calculates the centroid of the light spot based on the spot size. When the output response varies as a function of input intensity, edge detection and centroid

calculations are more difficult. In regions where a large change in intensity causes a lower than normal change in grey level, peak intensities will be attenuated to lower than appropriate grey levels. Thus, centroid calculation routines will not have the information about peaks, and the centroid will be miscalculated (Figure 5.2 a). This condition is seen near the saturation of the sensor. The inverse is true as well; when a small intensity produces a larger than normal change in grey level, points which should have almost the same grey level will have very different levels (Figure 5.2 b). Again, the centroid will be miscalculated. This condition is seen near the lowest threshold of the sensor.

Distortion due to non-linearity can displace centroids in any direction. In the case of the F/1.4 lens, the barrel distortion increased radially. Distortion due to non-linearity is compounded with the large lens barrel distortion component to give the overall distortion. The only information available to the image processing software is the resulting grey level in the captured image. Although a transformation could be developed which would map the measured grey levels to true grey levels, there will be information lost in areas where a large change in intensity results in a small change in grey level.

With respect to resolution, non-linearity makes line pairs difficult to discern because large changes in intensity can effect small changes in grey level which inhibits edge detection.

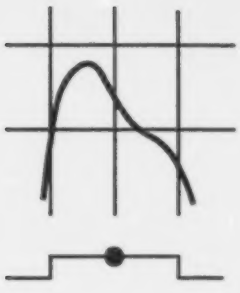

Scene

Quantized Image

• Centroid Calculation

a. Peak Intensity Attenuated

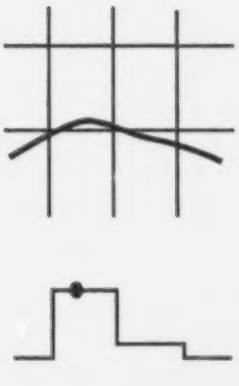

Scene

Quantized Image

• Centroid Calculation

b. Peak Intensity Magnified

Figure 5.2: Non-Linearity Effects on Centroid Calculation

Quantization

The number of quantization levels is very important for resolution. If contrast is low, black areas may be quantized to the same level as the white space between them. With more quantization levels, black and white areas will be quantized to different levels and the edges can be detected (Figure 5.3 a).

Quantization levels are also important for accurate centroid location. If there are more grey levels to indicate large intensity transitions then proper peak detection can be done and centroids accurately located (Figure 5.3 b).

Bloom

When sensing elements exhibit bloom, centroid localization is difficult because surrounding elements appear to be part of the object of interest. If bloom was symmetric in all directions it is possible that the centroid calculation for the imaged spot would coincide with the real spot. In this CCD sensor, the right neighbour received most of the excess charge. Consequently, high intensity point sources appear

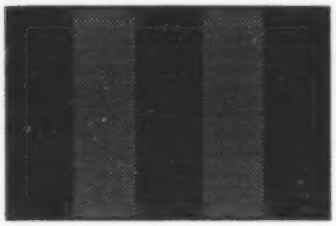

Scene

Few Quantization Levels

More Quantization Levels

a. More quantization levels allow better edge detection.

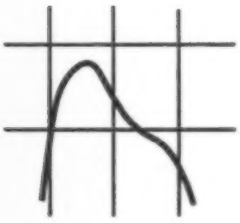

Scene

Few Quantization Levels

More Quantization Levels

• Centroid Calculation

b. More quantization levels allow proper peak detection and centroid calculations.

Figure 5.3: Quantization Level Effects on Centroid Calculation and Resolving Power

to be elongated toward the right, and centroids are miscalculated. This observation is supported by the fact that bloom usually occurs in the serial register before the parallel register (Epperson, 1987). Even before the sensing elements reach saturation, charge can diffuse in the direction of the horizontal line. This "tailing" effect also causes an elongation of point sources (Dähler, 1987). The cause is either the output register of the CCD sensor or the signal processing of the camera (Dähler, 1987).

Regarding resolution, bloom adds charge to sensing elements representing black areas. As a result, the modulation depth is decreased and edge detection is more difficult.

At the onset of saturation, this sensor bloomed 16.25 mV to its right neighbour and 4.1 mV to the other neighbours. These voltages at the sensor translate to 147 and 37 grey levels respectively at the frame grabber.

The effects of bloom are non-systematic. The amount of bloom varies depending on how over saturated the target sensing element is. A routine could be written which would detect if a pixel is in saturation, then adjust the surrounding pixel grey levels by an appropriate amount. This routine may alter data which should not be altered. Thus, the calibration routine would introduce distortions.

Uniformity

If sensing elements have the same incident light, but, different output grey levels, centroid localization will be erroneous. Similarly, if sensing elements have different incident light, but, the same output grey levels centroid localization will be erroneous. This non-uniformity, in effect, reduces the number of quantization levels available, and causes distortion and limits resolution. The reasons why quantization levels limit accuracy were discussed previously.

Non-uniformity of sensor response is systematic. Because sensing element non-uniformity is a function of incident light level, discrete levels of incident light across the entire dynamic range of the CCD must be used to analyze the change in grey level required for each pixel site. This change in grey level must be applied to the surface topography images on a pixel by pixel basis. This calibration will generate appropriate values for intensity level, however, some information on detail will already be lost.

5.4 Camera Circuitry

The aspect ratio mismatch caused a maximum distortion of 3 pixels (3.2 mm in object space). This aspect ratio also had consequences on image resolution. On the charts

used to determine distortion a horizontal line was imaged as 3 pixels wide, while a vertical line was imaged as 5 pixels wide. The 3 to 5 ratio may be due to the aspect ratio mismatch of the system. Electronic filter ripple which results in the output of one sensing element spreading over five sensing elements worth of time could be responsible. Furthermore, there was a shadow of a line two pixels to the right of the imaged vertical lines. This shadow was evident in the captured image, on video monitors and on an oscilloscope. Overshoots are often designed into the signal processing for edge enhancement, however, when they are too strong, they produce multiple reproductions of objects (Dähler, 1987).

The CCD sensing elements exhibited a near linear output response to incident light intensity (Figure 4.4). However, the signal processing stage transforms that response into an exponential response (Figure 4.5). The effects on distortion and resolution due to non-linearity were addressed previously regarding sensor linearity.

5.6 Summary

The most significant contribution to overall distortion is from the lens barrel distortion (3.2 mm). The spatial variation of the output response with respect to the input response introduces an uncertainty of 0.5 mm. Digitizing an irregular shape

into a regular pattern causes 0.1 mm point localization error. However, this can be reduced by decreasing the sensing element pitch or increasing the control point size. The most significant limitation on resolving power is the sensing element pitch. Lens diffraction (0.5 mm) and chromatic abberation (1.5 mm) de-focuses imaged points and decreases resolving power. Sensor spectral response, non-linearity, bloom, and non-uniformity, cause grey levels to be higher or lower than expected for some picture elements. However, the effect on point localization is not significant unless sub-pixel approximation techniques are used.

Although not investigated, the signal processing and the frame grabber circuitry, also distort the signal. Besides the 3.2 mm distortion due to aspect ratio, the long time constant which causes the point spread and the filter which causes the ringing may cause significant errors. In addition, the non-linear behaviour of the signal processing stage cause errors which may be significant.

CHAPTER SIX: RECOMMENDATIONS AND CONCLUSIONS

At each stage of a video image capture system distortion is added to the original illumination information. Some distortions are easier to correct than others. The errors which are systematic can be accounted for in the image processing steps after the image data has been captured. Sources of non-systematic errors must be eliminated by replacement with another method, reduced in some way, or accepted.

6.1 Recommendations

Recommendations are categorized into the parts of the image capture system.

1) Object in Scene

There are two things regarding the patient's back that can be done to improve the acquired images. To eliminate the difficulty in obtaining light spots on the side images, the skin on the side of the patient's backs should first be treated with a reflective coating, such as the glitter spray used in theatrics. In this way, the side spots will reflect more light and these points will be more easily discernable from the background black level. The centre of the patient's back should not have reflective

coating since this may induce blooming effects.

Secondly, the light source used to illuminate the patient should be band limited to red. This will improve image quality in two ways: the effect of chromatic abberation of the lens will be eliminated and the CCD responds more efficiently to red light.

2) Lens

One common action to decrease abberation effects is to stop down the lens so that the edges of the lens are not used. In this way, the barrel distortion and other abberations described in Chapter 2 can be decreased. Stopping down offers another benefit to the topography system: the depth of focus will increase. One disadvantage is that diffraction increases with f-stop so that the Airy disk size will increase; thus, decreasing resolution. The best value for f-stop should be determined through trial and error with a line pairs/mm resolution chart. The intensity of the light source for light spot projection must be increased as f-number is increased since light passing power of a lens is inversely proportional to f-number.

The illumination intensity of light spots at the periphery of the image should be brighter than those at the centre. This will counteract $\cos^4$ losses towards the edge of the lens, and provide a uniform image.

Both the radial and tangential distortion components should be incorporated the into calibration routines applied in the image processing steps (Sid-Ahmed, et al., 1990). Mathematical models from the values obtained for distortion in Chapter 3 or the parameters given by the survey technique described by Peterson et al. (in press) can be used in these routines.

If stopping down and calibration do not increase the accuracy of measurements, then another lens of a higher quality should be purchased. Lenz & Fritsch (1990) discuss appropriate lenses for use in videometry using CCD sensors.

3) CCD Sensor

Distortions due to the CCD sensor non-uniformity can be reduced by calibration routines implemented at the image processing stage. Distortions due to spectral response, non-linearity, and bloom are not systematic.

Future image capture systems should use a CCD sensor which will exhibit better performance characteristics. Several techniques have been implemented to improve on the performance of CCD sensors (Yamada & Fukumoto, 1989; Teranishi et al., 1987; Hopkinson & Lumb, 1982; Matsumoto, 1991; Hynecek, 1988). To improve the density of sensing elements a frame transfer CCD should be used instead of an interline transfer CCD. On interline transfer arrays, the sensing and read-out areas

are interspaced. On frame transfer arrays, one half of the CCD is sensing area and the other half is read-out area, thus, there is no gap between sensing elements. In addition, the CCD sensor should have external control over integration time, so, image smear due to patient sway and breathing can be eliminated.

An anti-aliasing technique described by Kazunori and Murakami (1983) or Kriss (1990) should be used to eliminate spatial aliasing due to sensor geometrical limitations.

4) Signal Processing

The horizontal:vertical aspect ratio should be adjusted to equal 1:1. Although NTSC standards dictate that the horizontal scanning frequency should be 15.75 kHz, this is not appropriate for this surface topography system. If this unequal aspect ratio is eliminated then calibration parameters for lens correction will apply in all directions, simplifying the calibration procedure.

In these experiments the largest source of error was the signal processing performed by the camera. Translation into an NTSC signal deforms the scene information significantly. In particular, the ringing exhibited after high light intensity is detected caused smear and shadowing. The most accurate use of a CCD sensor would be to

transfer the sensor analog output directly into a data acquisition board.

5) Frame-Grabber

The number of quantization levels should be increased. The Scion II frame grabber is only capable of 8 bits of quantization levels while 12 bits are now common.

The number of horizontal and vertical pixels of the frame grabber should be equivalent to the number of sensing elements of the sensor. In this way, there is a one to one ratio, and information will not be lost due to sampling error.

The source of synchronization signal for the camera used in the surface topography system could be adjusted between external, line, and internal. Unfortunately, there is no method to externally synchronize the frame grabber. Synchronized systems where the camera sel-clock is used to trigger the A/D converter pixel-clock would be very advantageous as it would eliminate the jitter due to mismatched synchronization pulses (Reimar & Fritsch, 1990; Dähler, 1987).

6) Image Processing

The systematic errors discussed so far should be incorporated into calibration routines performed on the two dimensional images of the surface topography system. Systematic distortions were: radial distortion, tangential distortion, and uniformity. Several investigators have suggested methods for correcting distortions to obtain measurements from images which are within desired accuracy requirements (Cholewicki et al., 1991; Dijak, 1985; Yokobori et al., 1986; Butler & Pierson, 1991; Fryer et al., 1989; Fraser & Shortis, 1990).

The surface topography system image processing stage should incorporate a weighting function based on the grey level of the pixels when calculating light spot centroid location.

Finally, without sub-pixel approximation, this system will not attain more than 0.5 mm accuracy (one pixel represents approximately 1 mm in object space). The image processing stage should incorporate this approximation procedure after the systematic errors are removed from the data.

6.2 Conclusions

Overall system distortion was 5 pixels, maximum, at the periphery of the image, which in image space is 5.4 mm. The overall system resolution was 34 line pairs/mm, which in image space means line centres must be separated by 2.3 mm. Each stage of the surface topography system was investigated. Although not investigated in detail in this thesis, the signal processing stage seemed to contribute the most to system distortion and low resolution, mostly due to the long time constant trail-off of signals.

The F/1.4 lens used in this surface topography measurement system also exhibited significant distortion and resolution limiting properties. There was a significant barrel distortion which was reduced by using a F/3.5 lens. Diffraction and chromatic abberations were quantified, but, were less significant.

The CCD sensor is a very accurate measurement tool. Its most significant contribution to overall distortion is due to location uncertainty, it can only pinpoint locations with an accuracy of 0.5 mm in image space. The overall system resolution is primarily limited by the size of the sensing element pitch and sensitive area. The process of digitizing an irregular shape into a regular pattern does not contribute significantly to overall distortion. Sensor characteristics (non-linearity, bloom, uniformity, spectral response) contribute slightly to overall distortion, however, the

magnitude is less than in the other stages of the camera and is not significant unless subpixel approximation is used.

Systematic errors can be eliminated at the image processing stage. However, the errors which were non-systematic cause a significant loss of information about the scene.

6.3 Future Work

The sensitivity profile of the sensing elements should be measured. Although subpixel approximation programs can obtain satisfactory results assuming a rectangular response, the results will be more accurate with a more accurate response model.

The effect of patient sway and breathing on image smear should be investigated. For this investigation, integration time must be adjustable.

The image sensor should be investigated in more detail regarding noise, dark current and charge transfer efficiency. To do this, detailed specifications on the CCD sensor, CCD driving circuitry controllable by the user, and sensitive measuring equipment are necessary.

The feasibility of improving the density of spots in the light pattern should be investigated.

REFERENCES

Adams, W., 1865. Lectures on the Pathology and Treatment of Lateral and Other Forms of Curvature of the Spine. London: John Churchill & Sons.

Bailey, R., Damerell, C.J.S., English, R.L., Gillman, A.R., Lintern, A.L., Watts, S.J. and Wickens, F.J., 1982. First Measurement of Efficiency and Precision of CCD Detectors for High Energy Physics. Chilton, England: Science and Engineering Research Council. (NTIS No. PB83-255208)

BEAM 2: Optical Ray Tracer, 1986. (Computer Program). Berkeley, CA: Stellar Software.

Beynon, J.D.E. and Lamb, D.R. (Eds.), 1980. Charge-Coupled Devices and Their Applications. McGraw-Hill Book Company, Maidenhead, England.

Boyle, W.S. and Smith, G.E., 1970. Experimental Verification of the Charge-Coupled Device Concept. Bell Systems Technical Journal, 49, 593-600.

Burwell, R.G., 1992. 3-D Etiological and Prognostic Aspects of Scoliotic Deformities. International Symposium of 3-D Scoliotic Deformities, (pp. 182-192). Montreal, Canada: Ecole Polytechnique.

Butler, D.A. and Pierson, P.K., 1991. A Distortion-Correction Scheme for Industrial Machine-Vision Applications. IEEE Transactions on Robotics and Automation, 7(4), 546-551.

Chih-Shing, H., 1983. Precision of Digital Vision Systems. Transactions on Pattern Analysis and Machine Intelligence, PAMI-5(6), 593-601.

Cholewicki, J., McGill, S.M., Wells, R.P., and Vernon, H., 1991. Method for Measuring Vertebral Kinematics from Videofluoroscopy. Clinical Biomechanics, 6, 73-78.

Dähler, J., 1987. Problems in Digital Image Acquisition with CCD Cameras. Proc. ISPRS Intercommission Conference on Fast Processing of Photogrammetric Data, Interlaken, Switzerland, 48-59.

Damerell, C.J.S., English, R.L., Gillman, A.R., Lintern, A.L., and Wickens, F.J., 1986. Use of Charge-Coupled Devices as High Precision Detectors. IEEE Transactions on Nuclear Science, 33(1), 51-53.

Dijak, J.T., 1985. A Method for Correcting Geometric Distortion in Video Cameras. IEEE Proceedings of the National Aerospace and Electronics Conference, 1382-1388.

Drerup, B., 1992. 3-D Acquisition, Reconstruction and Modelling Techniques Applied on Scoliotic Deformities. International Symposium of 3-D Scoliotic Deformities, (pp. 2-10). Montreal, Canada: Ecole Polytechnique.

Dubousset, J., 1992. Importance of the Three-Dimensional Concept in the Treatment of Scoliotic Deformities. International Symposium of 3-D Scoliotic Deformities, (pp. 302-311). Montreal, Canada: Ecole Polytechnique.

El-hakim, S.F., Burner, A.W., and Real, R.R, 1989. Video Technology and Real-Time Photogrammetry. In H.M. Karara (Ed.), Non-Topographic Photogrammetry (2nd ed.) (pp. 279-304). Church Falls, VA: American Society for Photogrammetry and Remote Sensing.

EG&G Photon Devices, July 1989. Photodiodes. (Catalog).

Epperson, P.M., 1987. Application and Characterization of Charge-Coupled Device Array Detectors for Analytical Spectroscopy. Dissertation Abstracts International, 48, 12-B.

Fabian, M.E., 1981. Semiconductor Laser Diodes; A Users Handbook. Electrochemical Publications Limited, Scotland.

Fedotov, M.G., Kuper, E.A., Panchenko, V.E., and Tiunov, S.A., 1989. Spatial distortions in solid-state semiconductor imagers in x-ray region. Rev. Sci. Instrum., 60(7), 2333.

Fraser, C.S. and Shortis, M.R., 1990. A Correction Model for Variation of Distortion Within the Photographic Field. SPIE: Close-Range Photogrammetry Meets Machine Vision, 1395, 244-251.

Frobin, W. and Hierholzer, E., 1981. Rasterstereography: A Photogrammetric Method for Measurement of Body Surfaces. Photogrammetric Engineering and Remote Sensing, 47(12), 1717-1724.

Frobin, W. and Hierholzer, E., 1983. Automatic Measurement of Body Surfaces Using Rasterstereography, Part I: Image Scan and Control Point Measurement. Photogrammetric Engineering and Remote Sensing, 49(3), 377-384.

Fryer, J.G., 1986. Lens Distortion for Close-Range Photogrammetry. Photogrammetric Engineering and Remote Sensing, 52(1), 51-58.

Fryer, J.G., 1989. Camera Calibration in Non-Topographic Photogrammetry. In H.M. Karara (Ed.), Non-Topographic Photogrammetry, (2nd ed.) (59-68). Church Falls, VA: American Society for Photogrammetry and Remote Sensing.

Fryer, J.G. and Mason, S.O., 1989. Rapid Lens Calibration of a Video Camera, Photogrammetric Engineering and Remote Sensing, 55(4), 437-442.

Glanze, W.D. (Ed.), 1985. The Mosby Medical Encyclopedia. New York: New American Library.

Hakkarainen, J., 1986. Effect of Light Wavelength on Distortion. Progress in Imaging Sensors, Proc. ISPRS Symposium, ESA SP-252, 355-356.

Halliday, D., and Resnick, R., 1981. Fundamentals of Physics, (2nd ed.). New York: John Wiley & Sons, Inc.

Havelock, David I., 1989. Geometric Precision in Noise-Free Digital Images. IEEE Transactions on Pattern Analysis and Machine Intelligence, 11(10), 1065-1075.

Hierholzer, E. and Drerup, B., 1992. Which Requirements Must Be Met in Order to Replace Radiography by Surface Topography? International Symposium of 3-D Scoliotic Deformities, (pp. 131-138). Montreal, Canada: Ecole Polytechnique.

Hill, D.L., Raso, V.J., Durdle, N.G., and Peterson, A.E., 1990. A Video Based Technique for Trunk Measurement. Sixth International Symposium on Surface Topography and Spinal Deformity, Proceedings, 52-53.

Hill, D.L., Raso, V.J. Durdle, N.G., and Peterson, A.E., 1992. Designing a Video Based Technique for Trunk Measurement. International Symposium on 3-D Scoliotic Deformities, (157-161). Montreal, Canada: Ecole Polytechnique.

Ho, Chih-Shing, 1983. Precision of Digital Vision Systems. IEEE Transactions on Pattern Analysis and Machine Intelligence, PAMI-5(6), 593-601.

Hopkinson, G.R., and Lumb, D.H., 1982. Noise reduction techniques for CCD image sensors. J. Phys. E.: Sci. Instrum., 15, 1214-1222.

Hopkinson, G.R., 1987. Analytic Modelling of Charge Diffusion in Charge-Coupled-Device Imagers. Optical Engineering, 26(8), 766-772.

Hopkinson, G.R., Cockshott, R.A., Purell, D.J., Skipper, M.D., and Taylor, S., 1987. Operation, performance, and reliability testing of charge-coupled devices for star trackers, Optical Engineering, 26(8), 725-733.

Horder, A. (Ed.), 1971. The Manual of Photography. Focal Press, New York.

Hutber, D., 1987. Improvement of CCD Camera Resolution using A Jittering Technique. SPIE: Automated Inspection and High Speed Vision Architectures, 849, 11-17.

Hynecek, J., 1988. A New Device Architecture Suitable for High-Resolution and High-Performance Image Sensors. IEEE Transactions on Electron Devices, 35(3), 646-652.

Jung, W.G., 1986. IC Op-Amp Cookbook (3rd Ed.). Howard W. Sams & Co., Indianapolis, IN.

IRE Standards on Video Techniques: Measurement of Resolution of Camera Systems, 1961. Proceedings of the IRE, 49(2), 600-602.

Kriss, M.A., 1990. Image Analysis of Discrete and Continuous Systems: Film and CCD Sensors. SPIE CAN-AM Eastern, 1398, 4-14.

Kiver, M.S., 1964. Color Television Fundamentals (2nd ed.). New York: McGraw-Hill Book Company.

Lenz, R. and Fritsch, D., 1990. Accuracy of Videometry with CCD Sensors, ISPRS Journal of Photogrammetry and Remote Sensing, 45, 90-110.

Li, Y., Young, T., and Huang, C., 1989. Noncontact Measurement Using Line-Scan Cameras: Analysis of Positioning Error. IEEE Transactions on Industrial Electronics, 36(4), 545-551.

Little, T.R., 1977. Real Time Digital Correction of Acquisition Errors Applied to Solid State Scanners. SPIE: Application of Digital Image Processing, (119), 173-181.

Matsumoto, K., Takayanagi, I., Nakamura, T. and Ohta, R., 1991. Analysis of Operational Speed and Scaling Down the Pixel Size of a Charge Modulation Device (CMD) Image Sensor. IEEE Transactions on Electron Devices, 38(5), 999-1004.

McCaughan, D.V. and Holeman, B.R., 1979. Applications of CCDs to Imaging. In Howes, M.J. and Morgan, D.V. (Ed.), Charge-Coupled Devices and Systems (pp. 241-292). Toronto, Canada: John Wiley and Sons Ltd.

Melles-Griot, 1988. Optics Guide. California: Author.

Mikhail, Edward M., McGlone, J. Chris, Paderes, and Fidel C., Jr., 1989. Introduction to Metrology Concepts. In H.M. Karara (Ed.), Non-Topographic Photogrammetry, (2nd Ed.) (pp. 7-14). Church Falls, VA: American Society for Photogrammetry and Remote Sensing.

Mori, C, Hirokane, M., 1989. Method and Accuracy of Stereoscopic Measurement Using a Camera with Linear Array CCD sensor. Proceedings of the Japan Society of Civil Engineers, 407, 37-45.

Neubart, J., 1987. Wide-angle Lenses in Perspective. Industrial Photography, January, 17-19.

Newport, 1990. Newport Catalog: Precision Laser & Optics Products. Mississauga, Ontario: Author.

Ohnishi, K. and Murakami, K., 1985. Sensitivity Distribution Measurement of Sensor Element for the Solid-State Imager. IEEE Transactions on Electron Devices, ED-32(8), 1417-1420.

Peterson, A.E., Durdle, N.G., Raso, V.J., and Hill, D.L., 1993. Calibration of Video Cameras for Scoliosis Mapping. Manuscript submitted for publication.

Rasband, W., 1990. Image: Image Processing and Analysis, Version 1.47 (Computer Program). Washington, D.C: National Institute of Health, Research Services Branch, NIMH.

Raso, V.J., Greenhill, B., Moreau, M.J., and Budney, D., 1986. The combined reconstruction of spinal and surface deformity. Surface Topography and Spinal Deformity, 13-20.

Real, R.R, 1986. Components for Video-Based Photogrammetry of Dynamic

Processes. International Archives of Photogrammetry and Remote Sensing, 26(5).

Regan, J.D. and Parrish, J.A., 1982. The Science of Photmedicine. Plenum Press, New York.

Rodger, R., 1980. Shape Measurement with Moire Topography. PhD Thesis, Exeter College.

Rodgers, R.L., 1974. Charge-Coupled Imager for 525-line Television. Digest of I.E.E.E. Intercon March '74, Session 2.

Sedra, A.S., and Smith, K.C., 1982. Micro-Electronic Circuits. New York, NY: CBS College Publishing.

Sid-Ahmed, M.A., and Boraie, M.T., 1990. Dual Camera Calibration for 3-D Machine Vision Metrology. IEEE Transactions on Instrumentation and Measurement, 39(3), 512-516.

Slupsky, S., 1988. A Video Digitizer for Scoliosis Studies. Masters Thesis, University of Alberta.

Society of Photo-optical Instrumentation Engineers, 1965. Basic Optics and Optical

Instruments (Vol. 1). California: Author.

Spencer, G.H., and Murty, M.V.R.K., 1962. General Ray-Tracing Procedure. Journal of the Optical Society of America, 52(6), 672-678.

Stanley, W.D., Dougherty, G.R., and Dougherty, R., 1984. Digital Signal Processing, (2nd ed.). Reston, Virginia: Reston Publishing Company.

Stokes, I., 1992. 3-D Spinal Deformity Measurement Methods and Terminology. International Symposium of 3-D Scoliotic Deformities, (pp. 236-243). Montreal, Canada: Ecole Polytechnique.

Suzuki, N., Ono, T., Tezuka, M., and Kamishi, S., 1992. Moiré Topography and Back Shape Analysis - Clinical Application. International Symposium of 3-D Scoliotic Deformities, (pp. 124-130). Montreal, Canada: Ecole Polytechnique.

Tanikawa, K., Ito, Y., & Sei, H., 1976. Evaluation of Dark Current Non-Uniformity in a CCD. Applied Physical Letters, 17, 111.

Taub, H. & Schilling, D, 1977. Digital Integrated Electronics. New York, NY: McGraw-Hill, Inc.

Teranishi, N., and Ishihara, Y., 1987. Smear Reduction in the Interline CCD Image Sensor. IEEE Transactions on Electron Devices, ED-34(5), 1052-1056.

Tsai, R.Y., 1987. A Versatile Camera Calibration Technique for High-Accuracy 3D Machine Vision Metrology Using Off-the-Shelf TV Cameras and Lenses. IEEE Journal of Robotics and Automation, RA-3(4), 323-344.

Turner-Smith, A.R. and Harris, J.D., 1986. ISIS - An Automated Shape Measurement and Analysis System. In Harris, J.D. and Turner-Smith, A.R. (Eds.), Surface Topography and Spinal Deformity, (pp. 31-38). Stuttgart: Gustav Fischer Verlag.

Wegner, J., 1985. Measurement of Scoliosis Deformity Using Moiré Topography. Masters Thesis, University of Alberta.

Welford, W.T, 1991. Useful Optics. Chicago, IL: The University of Chicago Press.

Wiesel, J., & Voegtle, T., 1986. Evaluation of a Solid State Camera for Photogrammetric Applications. Progress in Imaging Sensors, Proc. ISPRS Symposium, ESA SP-252, 405-408.

Winburn, D.C., 1987. What Every Engineer Should Know About Lasers. New York,

NY: Marcel Dekker, Inc.

Yamada, T., and Fukumoto, A., 1989. Trench CCD Image Sensor. IEEE Transactions on Consumer Electronics, 35(3), 360-367.

Yokobori, N., Yeh, P.S., and Rosenfeld, A., 1986. Sub-Pixel Geometric Correction of Pictures by Calibration and Decalibration. Proceedings IEEE International Conference on Robotics and Automation, 448-453.

Zhang, Y. and Liang, J., 1989. System of High Precision Laser Alignment Using the Technique of CCD Area Image Measurement. SPIE: Precision Engineering and Optomechanics, 1167, 209-218.